R. Vescovini, L. Dozio
Exact Refined Buckling Solutions for Laminated Plates Under Uniaxial and Biaxial Loads
Composite Structures, Vol. 127, 2015, p. 356-368
doi:10.1016/j.compstruct.2015.03.003

Exact Refined Buckling Solutions for Laminated Plates Under Uniaxial and Biaxial Loads

Riccardo Vescovini*and Lorenzo Dozio

Dipartimento di Scienze e Tecnologie Aerospaziali, Politecnico di Milano

Via La Masa 34, 20156 Milano, Italy

Abstract

This paper presents a unified Lévy-type solution procedure for the buckling analysis of both thin and thick composite plates under biaxial loads. The plates are simply-supported at two opposite edges, while the two remaining sides are subjected to any combination of simply-supported, clamped and free conditions. The problem is formulated in the context of a variable-kinematic formulation, offering the advantage of automatically handling theories of various order. Both layerwise and equivalent single layer theories are considered. The governing equilibrium equations are derived analytically from the Principle of Virtual Displacements (PVD), and are solved exactly referring to the Lévy-type procedure. The accuracy of the predictions is demonstrated by comparison with results available in literature, including exact 3D solutions. A comprehensive set of benchmark results is provided for plates subjected to different loading and boundary conditions and characterized by various width-to-thickness ratios.

Keywords: buckling; exact solutions; variable-kinematic theories; plates.

1 Introduction

Composite structures are widely used in aerospace, civil and marine applications. They are often required to operate under loading conditions that can promote elastic instability, such as in the case of uniaxial or biaxial compression. During the design phase, buckling loads can be predicted with various approaches, including numerical, analytical and semi-analytical techniques. Often, ad-hoc tools are developed to improve the design process, making necessary the availability of reference solutions to check the accuracy of the results and validate new methods.

In general, exact buckling solutions can be derived for a limited set of stacking sequences, loading and boundary conditions. The Navier method can be applied to study cross-ply rectangular plates, simply-supported

*Corresponding author. *Email address:* riccardo.vescovini@polimi.it (Riccardo Vescovini)

at the four edges, and subjected to biaxial compression. The method leads to a standard eigenvalue problem that can be solved in closed-form or numerically, depending on the underlying plate theory. Another approach is the Lévy method, which is suitable for rectangular plates with two parallel edges simply-supported, and any combination of free, simply-supported and clamped conditions at the two remaining edges. In this case, the buckling problem is reduced to the solution of a transcendental equation, whose solution is sought numerically. Other boundary and loading conditions can be studied referring to approximate solution procedures, the most common being the Ritz, Galerkin, and modified Galerkin methods.

The application of the Navier and Lévy methods to the analysis of thin composite plates is discussed in Ref. [1], where classical plate theory (CPT) is adopted. The application of approximate solution strategies to plates with various boundary conditions, including elastically restrained edges, is found in Ref. [2–4]. Thin plate solutions are a useful reference during the analysis of plates with relatively high values of width-to-thickness ratio. However, they are inadequate when moderately thick plates are of concern, and the contribution of transverse shear deformation is not negligible.

First-order shear deformation theory (FSDT) is the simplest approach to account for transverse shear deformations. It has been applied to the buckling analysis of moderately thick plates in several studies. For instance, exact closed-form solutions are derived by Liew and co-workers [5] for the buckling analysis of simply-supported composite plates under biaxial loads using the Navier method. Exact solutions have been derived also for isotropic [6] and cross-ply [1, 7, 8] plates under various boundary conditions, referring to the Lévy-type approach. One drawback related to FSDT is the need for shear correction coefficients, as the underlying kinematic assumptions imply constant transverse shear deformation.

The introduction of correction coefficients can be avoided by employing a mixed first-order deformation theory, as discussed by Zenkour [9]. In his work, the Galerkin method is applied and approximate buckling loads are derived for any combination of boundary conditions at the four edges.

Higher-order theories are an effective approach to deal with relatively thick plates and avoid the need for shear correction factors. The basic idea is to represent the displacement field along the thickness with a polynomial expansion. In most cases, the in-plane displacements are represented with a cubic expansion, while the out-of-plane displacement is assumed to be quadratic at most. Exact buckling solutions are obtained by Reddy and Phan [10] for simply-supported plates applying the Navier method, while Hadian and Nayfeh [11] derive Lévy-type solutions for cross-ply laminates, using the state-space approach together with the method of orthonormalization.

Another application of the Lévy-type approach to high-order theories is found in the works of Khdeir [12–14] where biaxial buckling of symmetric and unsymmetric laminated plates is investigated for different boundary conditions. However, boundary conditions do not properly account for the effect of in-plane loads, as observed in Refs. [6, 8].

Shufrin and Eisenberger [15] present a procedure based on the extended Kantorovich method, referring to first-order and Reddy's high-order deformation theories. Buckling loads are derived for different kind of loading and boundary conditions. In the case of two parallel simply-supported edges and biaxial loading

condition, the solutions are exact.

Numerical solutions using collocation with radial basis functions and third-order shear deformation theory are presented by Ferreira et al. [16] for the uniaxial and biaxial buckling of laminated plates.

Isotropic plates, simply-supported along the four edges and subjected by pure compression, are studied by Matsunaga [17, 18] in the context of a two-dimensional higher-order theory, based on the method of power series expansion. The approach is particularly suited for the study of very thick plates.

Recently, a two variable refined theory [19] has been proposed to guarantee a quadratic variation of the transverse shear strain along the thickness, thus avoiding the use of a shear correction factor as required in FSDT theory. The theory enforces the satisfaction of the null traction boundary condition at the top and the bottom of the panel, and offers the advantage of leading to governing equations similar to those obtained in the context of CPT. The application of the two variable refined theory is discussed by Kim et al. [20] and Thai and Kim [21] with regard to the biaxial buckling of both isotropic and orthotropic plates. Exact solutions are derived using the Navier and Lévy methods, respectively.

A relatively limited amount of works in the literature regards the derivation of exact buckling solutions in the context of 3D elasticity theory and, in any case, they are restricted to the boundary conditions of simple-support at the four edges. An example is provided by the works of Srinivas and Rao [22], where buckling solutions are reported for cross-ply plates under pure and biaxial compression. Cross-ply plates are studied also by Noor [23], where 3D governing equations are solved using a high-order finite difference scheme. Solutions to the 3D problem are reported in a closed-form manner by Wittrick [24] for isotropic plates loaded in compression. More recently, a 3D approach has been proposed by Gu and Chattopadhyay [25] where buckling of laminated plates is reduced to the solution of a nonlinear eigenvalue problem.

The main restriction to the use of 3D theory is the time to derive the solutions, which can be not adequate in the context of sensitivity or parametric studies.

A powerful approach to automatically consider several plate theories within the same theoretical framework is the unified formulation proposed by Carrera [26, 27], often referred to as Carrera unified formulation (CUF). This technique relies on hierarchically-ordered approximations to describe the displacement field in the thickness direction, and allows to range from classical 2D to quasi-3D layerwise models. It follows that low-order theories can be used when thin plates are of concern, while high-order approximations can be adopted to study thicker plates. Concerning buckling problems, variable-kinematic theories have been applied by D'Ottavio and Carrera [28] to study the instability of plates and shells under biaxial loads. Exact solutions are derived with the Navier solution, and are restricted to boundary conditions of simple-support at the four edges. An extension to the buckling of anisotropic plates under various kind of loading and boundary conditions is provided by Fazzolari and Carrera [29] and Nali and Carrera [30]. In both cases, the solutions are not exact, as they are derived from the approximate solution of the governing equations by means of the Ritz, Galerkin, generalized Galerkin methods [29] and the finite element method [30].

To the best of the authors' knowledge, no exact solutions are available in the literature for the biaxial buckling of flat plates under various boundary condition, based on the variable-kinematic theory. A formulation

is here presented to obtain the exact buckling solutions for plates with two parallel edges simply-supported, and the two remaining edges subjected to any combination of clamped, free and simply-supported edges. Governing equations are derived from the Principle of Virtual Displacements (PVD), which is formulated in a fully nondimensional manner, and are successively solved referring to the Lévy-type procedure in conjunction with the state-space approach. The strain-displacement relation is modeled by using the Green-Lagrange expression, with and without the von Kármán approximation. The results are compared with those available in the literature, including exact three-dimensional solutions, revealing excellent accuracy. A number of results is finally reported for different boundary conditions and loading conditions to be used in the future for benchmarking purposes.

2 Plate description

A multilayered rectangular plate is considered, as illustrated in Figure 1. The plate is obtained by the stacking of an arbitrary number N_l of orthotropic layers, each of them characterized by a thickness h_k and subjected to a three-dimensional state of stress. It is assumed that the layers are perfectly bonded along the common surfaces, so that interlaminar compatibility of the displacements is implied. The plate has length a, width b and total thickness equal to h.

In the present formulation, two classes of theories of order N are considered, namely the equivalent single-layer displacement-based (EDN) and the layerwise displacement-based (LDN) theories [27]. In the former, one single reference system is taken on the midsurface of the laminate, as sketched in Figure 2(a); in the latter, a number of N_l reference systems are taken on the midsurfaces of each single ply, as illustrated in Figure 2(b). In both cases, the z-axis is directed along the normal to the plate, while the x-axis is parallel to the plate longitudinal edges of length a, and the y-axis forms a right-handed system.

As depicted in Figure 1, the two edges at $y = 0, b$ are assumed to be simply-supported, while the two remaining parallel edges are constrained with any combination of free (F), simply-supported (S) and clamped conditions (C).

The panel is subjected to biaxial loads, consisting in the forces per unit length N_x and N_y, taken positive in traction, along the longitudinal and the transverse directions, respectively. Defining σ^k_{0xx} and σ^k_{0yy} the pre-buckling stresses of the layer k, the stress resultants along the thickness are defined as:

$$N_x = \sum_{k=1}^{N_l} \int_{z_k}^{z_{k+1}} \sigma^k_{0xx} dz \qquad N_y = \sum_{k=1}^{N_l} \int_{z_k}^{z_{k+1}} \sigma^k_{0yy} dz \tag{1}$$

where z_k and z_{k+1} are the coordinate of the bottom and the top of the ply k, respectively.

In the present formulation, pre-buckling loads can be introduced by direct application of the stresses $\sigma^k_{0\alpha\alpha}$ at the boundaries, or with an imposed end shortening. The differences between these approaches are discussed hereinafter.

3 Principle of Virtual Displacements

The equilibrium equations of the multilayered panel are derived from the application of the Principle of Virtual Displacements. For the plate of Figure 1, the principle reads:

$$\sum_{k=1}^{N_l} \int_\Omega \int_{z_k}^{z_{k+1}} \left(\delta {\boldsymbol{\epsilon}_p^k}^{\mathrm{T}} \boldsymbol{\sigma}_p^k + \delta {\boldsymbol{\epsilon}_n^k}^{\mathrm{T}} \boldsymbol{\sigma}_n^k + \lambda \delta {\boldsymbol{\epsilon}_{p_{nl}}^k}^{\mathrm{T}} \boldsymbol{\sigma}_{p0}^k \right) dz d\Omega = 0 \tag{2}$$

where Ω is the reference surface, and is defined in the domain $[0,\, a] \times [0,\, b]$.

The first two terms of Eq. (2) are the internal work contributions due to the in-plane and normal stresses. The components of the stress vectors read:

$$\boldsymbol{\sigma}_p^k = \left\{ \sigma_{xx}^k \quad \sigma_{yy}^k \quad \tau_{xy}^k \right\}^{\mathrm{T}} \qquad \boldsymbol{\sigma}_n^k = \left\{ \tau_{xz}^k \quad \tau_{yz}^k \quad \sigma_{zz}^k \right\}^{\mathrm{T}} \tag{3}$$

and the corresponding work-conjugated strain components are:

$$\boldsymbol{\epsilon}_p^k = \left\{ \epsilon_{xx}^k \quad \epsilon_{yy}^k \quad \gamma_{xy}^k \right\}^{\mathrm{T}} \qquad \boldsymbol{\epsilon}_n^k = \left\{ \gamma_{xz}^k \quad \gamma_{yz}^k \quad \epsilon_{zz}^k \right\}^{\mathrm{T}} \tag{4}$$

The third contribution of Eq. (2) is related to the pre-buckling condition, and is obtained as the product between the pre-buckling stress vector and the nonlinear part of the Green-Lagrange strain tensor. The scalar λ denotes the buckling multiplier. Considering only in-plane pre-buckling stresses, the vector $\boldsymbol{\sigma}_{p0}^k$ is:

$$\boldsymbol{\sigma}_{p0}^k = \left\{ \sigma_{0xx}^k \quad \sigma_{0yy}^k \quad 0 \right\}^{\mathrm{T}} \tag{5}$$

while the components of the vector $\boldsymbol{\epsilon}_{p_{nl}}^k$ are:

$$\boldsymbol{\epsilon}_{p_{nl}}^k = \left\{ \frac{1}{2} \left[\left(u_{,x}^2 + v_{,x}^2 \right) \varphi + w_{,x}^2 \right] \quad \frac{1}{2} \left[\left(u_{,y}^2 + v_{,y}^2 \right) \varphi + w_{,y}^2 \right] \quad \left(u_{,x} u_{,y} + v_{,x} v_{,y} \right) \varphi + w_{,x} w_{,y} \right\}^{\mathrm{T}} \tag{6}$$

where u, v and w are the three components of the displacement vector along the axes x, y and z, respectively. The comma followed by a coordinate denotes derivation with respect to that coordinate.

The scalar φ is null if von Kármán approximation is adopted, and is equal to one otherwise. This term allows to automatically switch from von Kármán approximation, where only the nonlinear contribution due to the deflection w is considered, to a plate theory, herein denoted as full nonlinear, where also the nonlinear contributions due to the in-plane displacement components u and w are accounted for.

The stress-strain relation, under the assumption of linearly elastic material, is expressed as:

$$\begin{Bmatrix} \boldsymbol{\sigma}_p^k \\ \boldsymbol{\sigma}_n^k \end{Bmatrix} = \begin{bmatrix} \mathbf{C}_p^k & \mathbf{C}_{pn}^k \\ {\mathbf{C}_{pn}^k}^{\mathrm{T}} & \mathbf{C}_n^k \end{bmatrix} \begin{Bmatrix} \boldsymbol{\epsilon}_p^k \\ \boldsymbol{\epsilon}_n^k \end{Bmatrix} \tag{7}$$

where the components of the constitutive matrix, for an orthotropic ply oriented at 0° or 90°, are:

$$\mathbf{C}_p^k = \begin{bmatrix} \tilde{C}_{11}^k & \tilde{C}_{12}^k & 0 \\ \tilde{C}_{12}^k & \tilde{C}_{22}^k & 0 \\ 0 & 0 & \tilde{C}_{66}^k \end{bmatrix} \qquad \mathbf{C}_{pn}^k = \begin{bmatrix} 0 & 0 & \tilde{C}_{13}^k \\ 0 & 0 & \tilde{C}_{23}^k \\ 0 & 0 & 0 \end{bmatrix} \qquad \mathbf{C}_n^k = \begin{bmatrix} \tilde{C}_{55}^k & 0 & 0 \\ 0 & \tilde{C}_{44}^k & 0 \\ 0 & 0 & \tilde{C}_{33}^k \end{bmatrix} \tag{8}$$

4 Pre-buckling stress analysis

In the context of the buckling analysis, the stress components of Eq. (5) define an initial equilibrium condition whose stability is investigated. Based on previous works in the literature, three distinct approaches are here considered to determine the pre-buckling configuration. The first one consists in assuming an imposed uniform stress distribution over the laminate thickness. The second and the third strategies are related to the assumption of imposed end strains, and determine a stress distribution proportional to the stiffness of the layers, with and without deformation compatibility requirements, respectively.

Depending on the approach to compute the pre-buckling condition, the resultants $N_{\alpha\alpha}$ of Eq. (1) will be denoted as $N^{\sigma}_{\alpha\alpha}$, $N^{\epsilon}_{\alpha\alpha}$ or $N^{\varepsilon}_{\alpha\alpha}$.

4.1 Imposed uniform stress

The most common approach consists in assuming an imposed stress at the plate edges, and a corresponding pre-buckling stress distribution constant over the thickness of the laminate. The pre-buckling stress is then:

$$\sigma^{k}_{0xx} = P_x \quad \sigma^{k}_{0yy} = P_y \tag{9}$$

where P_x and P_y are the applied stresses at the longitudinal and transverse edges, respectively. In this case, the stress resultant over thickness are denoted as N^{σ}_{x} and N^{σ}_{y}.

From the elastic constitutive law of Eq. (7), the stress distribution of Eq. (9) is associated to a strain field proportional to the elastic coefficients of the layer. For a generic composite plate, the strains will be different from layer to layer, thus leading to interlaminar displacement discontinuity.

4.2 Imposed strain

A second approach, often found in the literature, consists in assuming an imposed uniform strain. In this case, all the layers are subjected to the same strain field and the pre-buckling stress distributes according to the elasticity coefficient of the layers. In the works of Refs. [23, 28], the stress distribution is calculated as:

$$\sigma^{k}_{0xx} = \tilde{C}^{k}_{11}\epsilon_{0xx} \quad \sigma^{k}_{0yy} = \tilde{C}^{k}_{22}\epsilon_{0yy} \tag{10}$$

where ϵ_{0xx} and ϵ_{0yy} are the imposed strains, which are constant for all the layers. In this case, the stress resultant over the thickness are denoted as N^{ϵ}_{x} and N^{ϵ}_{y}.

From the stress-strain relation of Eq. (7), it can be observed that Poisson's effects are neglected in the pre-buckling condition of Eq. (10). It follows that deformation compatibility between the layers is not ensured unless the material is isotropic or the plate is composed by one single layer.

4.3 Imposed compatible strain

A different approach is here proposed to guarantee interlaminar compatibility while imposing a uniform pre-buckling strain. An initial state is assumed, where the opposite edges are compressed by two rigid blocks,

translating each other with no rotation. The imposed strains are denoted as ϵ_{0xx} and ϵ_{0yy}.

The pre-buckling stress distribution is obtained from the ply constitutive law of Eq. (7) and imposing vanishing normal stress σ^k_{0zz}:

$$\begin{aligned}\sigma^k_{0xx} &= \tilde{C}^k_{11}\epsilon_{0xx} + \tilde{C}^k_{12}\epsilon_{0yy} + \tilde{C}^k_{13}\epsilon^k_{0zz}\\ \sigma^k_{0yy} &= \tilde{C}^k_{12}\epsilon_{0xx} + \tilde{C}^k_{22}\epsilon_{0yy} + \tilde{C}^k_{23}\epsilon^k_{0zz}\\ \sigma^k_{0zz} &= \tilde{C}^k_{13}\epsilon_{0xx} + \tilde{C}^k_{23}\epsilon_{0yy} + \tilde{C}^k_{33}\epsilon^k_{0zz} = 0\end{aligned} \tag{11}$$

The pre-buckling normal strain ϵ^k_{0zz} of the ply k can be expressed as a function of the applied in-plane strains from the third of Eq. (11). Substituting back ϵ^k_{0zz} into the first two of Eq. (11), the in-plane stresses are obtained as:

$$\begin{aligned}\sigma^k_{0xx} &= \left(\tilde{C}^k_{11} - \frac{\tilde{C}^{k\,2}_{13}}{\tilde{C}^k_{33}}\right)\epsilon_{0xx} + \left(\tilde{C}^k_{12} - \frac{\tilde{C}^k_{13}\tilde{C}^k_{23}}{\tilde{C}^k_{33}}\right)\epsilon_{0yy}\\ \sigma^k_{0yy} &= \left(\tilde{C}^k_{12} - \frac{\tilde{C}^k_{13}\tilde{C}^k_{23}}{\tilde{C}^k_{33}}\right)\epsilon_{0xx} + \left(\tilde{C}^k_{22} - \frac{\tilde{C}^{k\,2}_{23}}{\tilde{C}^k_{33}}\right)\epsilon_{0yy}\end{aligned} \tag{12}$$

For a multiaxial loading condition, where both the strains ϵ_{0xx} and ϵ_{0yy} are specified, the stress distribution is readily obtained from Eq. (12). In this case, the thickness resultants are denoted as N^ε_x and N^ε_y.

If a uniaxial loading condition is sought, i.e. only ϵ_{0xx} is imposed, the pre-buckling strain ϵ_{0yy} should be determined such that the resultant of the stresses σ^k_{0yy} along the thickness is null. This is done by imposing:

$$\begin{Bmatrix} N^\varepsilon_x \\ 0 \end{Bmatrix} = \begin{bmatrix} A_{11} & A_{12} \\ A_{12} & A_{22} \end{bmatrix} \begin{Bmatrix} \epsilon_{0xx} \\ \epsilon_{0yy} \end{Bmatrix} \tag{13}$$

where the terms A_{ik} are the in-plane stiffness coefficients of the laminate, obtained as:

$$A_{11} = \sum_{k=1}^{N_l}\left(\tilde{C}^k_{11} - \frac{\tilde{C}^{k\,2}_{13}}{\tilde{C}^k_{33}}\right)h_k \quad A_{12} = \sum_{k=1}^{N_l}\left(\tilde{C}^k_{12} - \frac{\tilde{C}^k_{13}\tilde{C}_{23}}{\tilde{C}^k_{33}}\right)h_k \quad A_{22} = \sum_{k=1}^{N_l}\left(\tilde{C}^k_{22} - \frac{\tilde{C}^{k\,2}_{23}}{\tilde{C}^k_{33}}\right)h_k \tag{14}$$

From Eq. (13), the pre-buckling transverse strain is:

$$\epsilon_{0yy} = -\frac{A_{12}}{A_{22}}\epsilon_{0xx} \tag{15}$$

The pre-buckling stress distribution is finally derived after substitution of Eq. (15) into Eq. (12).

5 Nondimensional parameters

A nondimensional formulation of the problem is developed after introducing proper dimensionless quantities, here denoted by an overline. The system $\overline{x}$-$\overline{y}$-$\overline{z}$ is defined, and the relation with the dimensional coordinates x-y-z is:

$$x = \overline{x}a \qquad y = \overline{y}b \qquad z = \overline{z}\frac{\widehat{h}}{2} \tag{16}$$

The coordinates $\overline{x}$ and $\overline{y}$ are normalized with respect to plate length and width, and vary in the interval $[0 \quad 1]$. The normal coordinate $\overline{z}$ is scaled with respect to the measure of thickness $\widehat{h}$, which is dependent on the plate theory considered. In particular, it is defined as as:

$$\begin{aligned}\widehat{h} &= h \quad \text{for EDN theory}\\ \widehat{h} &= h_k \quad \text{for LDN theory}\end{aligned} \tag{17}$$

The following relation is introduced for the elastic coefficients:

$$\tilde{C}_{ik} = E_2 \frac{h}{a} \overline{C}_{ik} \tag{18}$$

where the subscript ik denotes the generic component of the elasticity tensor, and E_2 is the transverse Young's modulus of the material. For plates obtained by the stacking of plies of different materials, the choice of E_2 is arbitrary.

The relation between the stresses and their dimensional counterpart is:

$$\sigma_{ik} = E_2 \left(\frac{h}{a}\right)^2 \overline{\sigma}_{ik} \tag{19}$$

The three components of the displacement are normalized with respect to the total thickness of the panel:

$$u = \overline{u}h \quad v = \overline{v}h \quad w = \overline{w}h \tag{20}$$

Finally, the pre-buckling multiplier λ, which is already a nondimensional quantity, is scaled as:

$$\lambda = \frac{a}{h}\overline{\lambda} \tag{21}$$

6 Nondimensional Principle of Virtual Displacements

According to the nondimensional terms introduced in the previous section, the Principle of Virtual Displacements of Eq. (2) can be recast in the form:

$$\sum_{k=1}^{N_l} \int_{\overline{\Omega}} \int_{\overline{z}_k}^{\overline{z}_{k+1}} \left(\delta \overline{\boldsymbol{\epsilon}}_p^{k^{\mathrm{T}}} \overline{\boldsymbol{\sigma}}_p^k + \delta \overline{\boldsymbol{\epsilon}}_n^{k^{\mathrm{T}}} \overline{\boldsymbol{\sigma}}_n^k + \overline{\lambda} \delta \overline{\boldsymbol{\epsilon}}_{p_{nl}}^{k^{\mathrm{T}}} \overline{\boldsymbol{\sigma}}_{p0}^k \right) \frac{\widehat{h}}{h} d\overline{z} d\overline{\Omega} = 0 \tag{22}$$

where:

$$\overline{\boldsymbol{\sigma}}_p^k = \left\{ \overline{\sigma}_{\overline{x}\overline{x}}^k \quad \overline{\sigma}_{\overline{y}\overline{y}}^k \quad \overline{\sigma}_{\overline{x}\overline{y}}^k \right\}^{\mathrm{T}} \quad \overline{\boldsymbol{\sigma}}_n^k = \left\{ \overline{\tau}_{\overline{x}\overline{z}}^k \quad \overline{\tau}_{\overline{y}\overline{z}}^k \quad \overline{\sigma}_{\overline{z}\overline{z}}^k \right\}^{\mathrm{T}} \quad \overline{\boldsymbol{\sigma}}_{p0}^k = \left\{ \overline{\sigma}_{0\overline{x}\overline{x}}^k \quad \overline{\sigma}_{0\overline{y}\overline{y}}^k \quad 0 \right\}^{\mathrm{T}} \tag{23}$$

and:

$$\overline{\boldsymbol{\epsilon}}_p^k = \left\{ \overline{\epsilon}_{\overline{x}\overline{x}}^k \quad \overline{\epsilon}_{\overline{y}\overline{y}}^k \quad \overline{\gamma}_{\overline{x}\overline{y}}^k \right\}^{\mathrm{T}} \quad \overline{\boldsymbol{\epsilon}}_n^k = \left\{ \overline{\gamma}_{\overline{x}\overline{z}}^k \quad \overline{\gamma}_{\overline{y}\overline{z}}^k \quad \overline{\epsilon}_{\overline{z}\overline{z}}^k \right\}^{\mathrm{T}} \tag{24}$$

while the nonlinear term of the Green-Lagrange strain tensor, expressed in nondimensional form, is:

$$\overline{\boldsymbol{\epsilon}}_{p_{nl}}^{k^{\mathrm{T}}} = \left\{ \tfrac{1}{2} \left[\left(\overline{u}_{,\overline{x}}^2 + \overline{v}_{,\overline{x}}^2 \right) \varphi + \overline{w}_{,\overline{x}}^2 \right] \qquad \tfrac{1}{2} \left(\tfrac{a}{b} \right)^2 \left[\left(\overline{u}_{,\overline{y}}^2 + \overline{v}_{,\overline{y}}^2 \right) \varphi + \overline{w}_{,\overline{y}}^2 \right] \qquad \tfrac{a}{b} \left[\left(\overline{u}_{,\overline{x}} \overline{u}_{,\overline{y}} + \overline{v}_{,\overline{x}} \overline{v}_{,\overline{y}} \right) \varphi + \overline{w}_{,\overline{x}} \overline{w}_{,\overline{y}} \right] \right\}^{\mathrm{T}} \tag{25}$$

The relation between the nondimensional stresses and strains reads:

$$\begin{Bmatrix} \overline{\boldsymbol{\sigma}}_p^k \\ \overline{\boldsymbol{\sigma}}_n^k \end{Bmatrix} = \begin{bmatrix} \overline{\mathbf{C}}_p^k & \overline{\mathbf{C}}_{pn}^k \\ \overline{\mathbf{C}}_{pn}^{k^{\mathrm{T}}} & \overline{\mathbf{C}}_n^k \end{bmatrix} \begin{Bmatrix} \overline{\boldsymbol{\epsilon}}_p^k \\ \overline{\boldsymbol{\epsilon}}_n^k \end{Bmatrix} \tag{26}$$

where:

$$\overline{\mathbf{C}}_p^k = \begin{bmatrix} \overline{C}_{11}^k & \overline{C}_{12}^k & 0 \\ \overline{C}_{12}^k & \overline{C}_{22}^k & 0 \\ 0 & 0 & \overline{C}_{66}^k \end{bmatrix} \qquad \overline{\mathbf{C}}_{pn}^k = \begin{bmatrix} 0 & 0 & \overline{C}_{13}^k \\ 0 & 0 & \overline{C}_{23}^k \\ 0 & 0 & 0 \end{bmatrix} \qquad \overline{\mathbf{C}}_n^k = \begin{bmatrix} \overline{C}_{55}^k & 0 & 0 \\ 0 & \overline{C}_{44}^k & 0 \\ 0 & 0 & \overline{C}_{33}^k \end{bmatrix} \tag{27}$$

having transformed the elastic coefficients of Eq. (8) according to Eq. (18).

The nondimensional strains are related to the nondimensional displacements through the relations:

$$\overline{\boldsymbol{\epsilon}}_p^k = \overline{\mathbf{D}}_p \overline{\mathbf{u}}^k \qquad \overline{\boldsymbol{\epsilon}}_n^k = \overline{\mathbf{D}}_n \overline{\mathbf{u}}^k + \frac{2a}{\widehat{h}} \frac{\partial}{\partial \overline{z}} \overline{\mathbf{u}}^k \tag{28}$$

where the differential matrices $\overline{\mathbf{D}}_p$ and $\overline{\mathbf{D}}_n$ are:

$$\overline{\mathbf{D}}_p = \begin{bmatrix} (\cdot)_{,\overline{x}} & 0 & 0 \\ 0 & \frac{a}{b}(\cdot)_{,\overline{y}} & 0 \\ \frac{a}{b}(\cdot)_{,\overline{y}} & (\cdot)_{,\overline{x}} & 0 \end{bmatrix} \qquad \overline{\mathbf{D}}_n = \begin{bmatrix} 0 & 0 & (\cdot)_{,\overline{x}} \\ 0 & 0 & \frac{a}{b}(\cdot)_{,\overline{y}} \\ 0 & 0 & 0 \end{bmatrix} \tag{29}$$

and the vector of displacements $\overline{\mathbf{u}}^k$ is defined as:

$$\overline{\mathbf{u}}^k = \overline{\mathbf{u}}^k(\overline{x}, \overline{y}, \overline{z}_k) = \left\{ \overline{u}^k \quad \overline{v}^k \quad \overline{w}^k \right\}^{\mathrm{T}} \tag{30}$$

In view of the derivation of the equilibrium equations, the pre-stress contribution of Eq. (22) is re-organized in matrix form as:

$$\delta \overline{\boldsymbol{\epsilon}}_{p_{nl}}^{k^{\mathrm{T}}} \overline{\boldsymbol{\sigma}}_{p0}^k = \left(\overline{\mathbf{D}}_{nl} \, \delta \overline{\mathbf{u}}^k \right)^{\mathrm{T}} \overline{\boldsymbol{\Sigma}}_{0p}^{\mathrm{k}} \overline{\mathbf{D}}_{nl} \overline{\mathbf{u}}^k \tag{31}$$

where the differential matrix $\overline{\mathbf{D}}_{nl}$ is:

$$\overline{\mathbf{D}}_{nl} = \begin{bmatrix} (\cdot)_{,\overline{x}} & 0 & 0 \\ \frac{a}{b}(\cdot)_{,\overline{y}} & 0 & 0 \\ 0 & (\cdot)_{,\overline{x}} & 0 \\ 0 & \frac{a}{b}(\cdot)_{,\overline{y}} & 0 \\ 0 & 0 & (\cdot)_{,\overline{x}} \\ 0 & 0 & \frac{a}{b}(\cdot)_{,\overline{y}} \end{bmatrix} \tag{32}$$

and the pre-stress matrix, here restricted to the in-plane contributions, is:

$$\overline{\boldsymbol{\Sigma}}_{0p}^{\mathrm{k}} = \begin{bmatrix} \varphi \overline{\sigma}_{0\overline{x}\overline{x}}^k & 0 & 0 & 0 & 0 & 0 \\ 0 & \varphi \overline{\sigma}_{0\overline{y}\overline{y}}^k & 0 & 0 & 0 & 0 \\ 0 & 0 & \varphi \overline{\sigma}_{0\overline{x}\overline{x}}^k & 0 & 0 & 0 \\ 0 & 0 & 0 & \varphi \overline{\sigma}_{0\overline{y}\overline{y}}^k & 0 & 0 \\ 0 & 0 & 0 & 0 & \overline{\sigma}_{0\overline{x}\overline{x}}^k & 0 \\ 0 & 0 & 0 & 0 & 0 & \overline{\sigma}_{0\overline{y}\overline{y}}^k \end{bmatrix} \tag{33}$$

From Eq. (30) and using the definitions of Eqs. (32) and (33), it is straightforward to verify Eq. (31).

6.1 Variable-kinematic theories

Following the approach proposed by Carrera [26], the displacement field at the generic layer k is approximated as:

$$\overline{\mathbf{u}}^k(\overline{x}, \overline{y}, \overline{z}_k) = F_\tau(\overline{z}_k) \overline{\mathbf{u}}_\tau^k(\overline{x}, \overline{y}) \qquad \text{with} \qquad \tau = 0, ..., N \tag{34}$$

where the repeated index τ implies summation according to the Einstein's convention. The function F_τ depends on the coordinate $\overline{z}_k$, and describes the displacement along the thickness direction. The vector $\overline{\mathbf{u}}^k_\tau(\overline{x},\overline{y})$ collects the three components of the generalized displacements, and is function of the in-plane coordinates $\overline{x}$ and $\overline{y}$.

Different theories can be derived in the context of the variable-kinematic theory, depending on the expression of the function F_τ. A class of equivalent layer (ED) theories is derived by assuming:

$$F_\tau(\overline{z}_k) = \overline{z}^\tau \qquad \tau = 0, 1, \dots N \tag{35}$$

Layerwise theories (LD) are derived taking $\tau = t, b, r$ and $r = 2, ..., N$, and choosing the thickness function F_τ as:

$$F_t(\overline{z}_k) = \frac{1+\overline{z}_k}{2} \qquad F_b(\overline{z}_k) = \frac{1-\overline{z}_k}{2} \qquad F_r(\overline{z}_k) = P_r(\overline{z}_k) - P_{r-2}(\overline{z}_k) \tag{36}$$

where $P_r(\overline{z}_k)$ is the Legendre polynomial of order r. The functions F_b and F_t are unitary at the bottom and the top of ply, respectively, while the terms F_r are null. It follows that the generalized displacements $\overline{\mathbf{u}}^k_t(\overline{x},\overline{y})$ and $\overline{\mathbf{u}}^k_b(\overline{x},\overline{y})$ are the actual displacements at the top and the bottom of the ply, and interlaminar compatibility can be easily satisfied after imposing $\overline{\mathbf{u}}^k_t = \overline{\mathbf{u}}^{k+1}_b$ for $k = 1, ...N_l - 1$.

Independently on the plate theory, the expansion of Eq. (34) can be substituted into Eq. (28) to obtain:

$$\overline{\boldsymbol{\epsilon}}^k_p = F_\tau \overline{\mathbf{D}}_p \overline{\mathbf{u}}^k_\tau \qquad \overline{\boldsymbol{\epsilon}}^k_n = F_\tau \overline{\mathbf{D}}_n \overline{\mathbf{u}}^k_\tau + \frac{2a}{\widehat{h}} F_{\tau,\overline{z}} \overline{\mathbf{u}}^k_\tau \tag{37}$$

Similarly, the nondimensional stresses can be expressed as function of the generalized displacement vector $\overline{\mathbf{u}}^k_\tau$ by substitution of Eq. (37) into Eq. (26):

$$\begin{aligned} \overline{\boldsymbol{\sigma}}^k_p &= F_\tau \overline{\mathbf{C}}^k_{pp} \overline{\mathbf{D}}_p \overline{\mathbf{u}}^k_\tau + F_\tau \overline{\mathbf{C}}^k_{pn} \overline{\mathbf{D}}_n \overline{\mathbf{u}}^k_\tau + F_{\tau,\overline{z}} \frac{2a}{\widehat{h}} \overline{\mathbf{C}}^k_{pn} \overline{\mathbf{u}}^k_\tau \\ \overline{\boldsymbol{\sigma}}^k_n &= F_\tau \overline{\mathbf{C}}^{k\,\mathrm{T}}_{pn} \overline{\mathbf{D}}_p \overline{\mathbf{u}}^k_\tau + F_\tau \overline{\mathbf{C}}^k_n \overline{\mathbf{D}}_n \overline{\mathbf{u}}^k_\tau + F_{\tau,\overline{z}} \frac{2a}{\widehat{h}} \overline{\mathbf{C}}^k_n \overline{\mathbf{u}}^k_\tau \end{aligned} \tag{38}$$

The Principle of Virtual Displacements, in the context of the variable-kinematic theory here developed, is re-written substituting Eq. (37) into of Eq. (22):

$$\begin{aligned} \sum_{k=1}^{N_l} \int_{\overline{\Omega}} \int_{\overline{z}_k}^{\overline{z}_{k+1}} \Big[\left(\overline{\mathbf{D}}_p \delta \overline{\mathbf{u}}^k_\tau\right)^{\mathrm{T}} F_\tau \overline{\boldsymbol{\sigma}}^k_p + \left(\overline{\mathbf{D}}_n \delta \overline{\mathbf{u}}^k_\tau\right)^{\mathrm{T}} F_\tau \overline{\boldsymbol{\sigma}}^k_n + \delta \overline{\mathbf{u}}^{k\,\mathrm{T}}_\tau \frac{2a}{\widehat{h}} F_{\tau,\overline{z}} \overline{\boldsymbol{\sigma}}^k_n \\ + \overline{\lambda} \left(\overline{\mathbf{D}}_{nl} \delta \overline{\mathbf{u}}^k_\tau\right)^{\mathrm{T}} F_s F_\tau \overline{\boldsymbol{\Sigma}}^{\mathrm{k}}_{0p} \overline{\mathbf{D}}_{nl} \overline{\mathbf{u}}^k_s \Big] \frac{\widehat{h}}{h} d\overline{z} d\overline{\Omega} = 0 \end{aligned} \tag{39}$$

6.2 Equations in terms of stress resultants

Governing equilibrium equations are now derived in terms of stress resultants. To this aim, the stress integrals along the thickness are introduced as:

$$\begin{aligned} \overline{\mathbf{R}}^k_{p\tau} &= \begin{Bmatrix} \overline{R}^k_{\overline{x}\overline{x}\tau} \\ \overline{R}^k_{\overline{y}\overline{y}\tau} \\ \overline{R}^k_{\overline{x}\overline{y}\tau} \end{Bmatrix} = \int_{\overline{z}_k}^{\overline{z}_{k+1}} F_\tau \overline{\boldsymbol{\sigma}}^k_p \frac{\widehat{h}}{h} d\overline{z} \qquad \overline{\mathbf{R}}^k_{n\tau} = \begin{Bmatrix} \overline{R}^k_{\overline{x}\overline{z}\tau} \\ \overline{R}^k_{\overline{y}\overline{z}\tau} \\ \overline{R}^k_{\overline{z}\overline{z}\tau} \end{Bmatrix} = \int_{\overline{z}_k}^{\overline{z}_{k+1}} F_\tau \overline{\boldsymbol{\sigma}}^k_n \frac{\widehat{h}}{h} d\overline{z} \\ \overline{\mathbf{R}}^k_{n\tau_z} &= \begin{Bmatrix} \overline{R}^k_{\overline{x}\overline{z}\tau_z} \\ \overline{R}^k_{\overline{y}\overline{z}\tau_z} \\ \overline{R}^k_{\overline{z}\overline{z}\tau_z} \end{Bmatrix} = \int_{\overline{z}_k}^{\overline{z}_{k+1}} F_{\tau,\overline{z}} \overline{\boldsymbol{\sigma}}^k_n \frac{2a}{h} d\overline{z} \end{aligned} \tag{40}$$

From the definitions of Eq. (40) and recalling the expression of Eq. (39), the Principle of Virtual Displacements is re-written in terms stress resultants as:

$$\sum_{k=1}^{N_l} \int_{\overline{\Omega}} \left[\left(\overline{\mathbf{D}}_p \delta \overline{\mathbf{u}}_\tau^k\right)^{\mathrm{T}} \overline{\mathbf{R}}_{p\tau}^k + \left(\overline{\mathbf{D}}_n \delta \overline{\mathbf{u}}_\tau^k\right)^{\mathrm{T}} \overline{\mathbf{R}}_{n\tau}^k + \delta \overline{\mathbf{u}}_\tau^{k\,\mathrm{T}} \overline{\mathbf{R}}_{n\tau_z}^k + \overline{\lambda} \overline{J}_{\tau s}^k \left(\overline{\mathbf{D}}_{nl} \delta \overline{\mathbf{u}}_\tau^k\right)^{\mathrm{T}} \overline{\mathbf{\Sigma}}_{0p}^{\mathrm{k}} \overline{\mathbf{D}}_{nl} \overline{\mathbf{u}}_s^k \right] d\overline{\Omega} = 0 \tag{41}$$

where $\overline{J}_{\tau s}^k$ is the thickness integral of the functions F_τ and F_s and its expression is reported in the Appendix. The strong form formulation of the problem, in terms of equilibrium equations and boundary conditions, is derived after integrating by parts the functional of Eq. (41). The expression reads:

$$\begin{aligned} &-\sum_{k=1}^{N_l} \int_{\overline{\Omega}} \delta \overline{\mathbf{u}}_\tau^{k\,\mathrm{T}} \left(\overline{\mathbf{D}}_p^{\mathrm{T}} \overline{\mathbf{R}}_{p\tau}^k + \overline{\mathbf{D}}_n^{\mathrm{T}} \overline{\mathbf{R}}_{n\tau}^k - \overline{\mathbf{R}}_{n\tau_z}^k + \overline{\lambda} \overline{\mathbf{D}}_{nl}^{\mathrm{T}} \overline{\mathbf{\Sigma}}_{0p}^{\mathrm{k}} \overline{\mathbf{D}}_{nl} \overline{\mathbf{u}}_s^k \overline{J}_{\tau s}^k \right) d\overline{\Omega} \\ &+ \int_{\overline{\Gamma}} \delta \overline{\mathbf{u}}_\tau^{k\,\mathrm{T}} \left(\overline{\mathbf{I}}_p^{\mathrm{T}} \overline{\mathbf{R}}_{p\tau}^k + \overline{\mathbf{I}}_n^{\mathrm{T}} \overline{\mathbf{R}}_{n\tau}^k + \overline{\lambda} \overline{\mathbf{I}}_{nl}^{\mathrm{T}} \overline{\mathbf{\Sigma}}_{0p}^{\mathrm{k}} \overline{\mathbf{D}}_{nl} \overline{\mathbf{u}}_\tau^k \overline{J}_{\tau s}^k \right) d\overline{\Gamma} = 0 \end{aligned} \tag{42}$$

where $\overline{\Gamma}$ is the boundary to the domain $\overline{\Omega}$, and the matrices $\overline{\mathbf{I}}_p$, $\overline{\mathbf{I}}_n$ and $\overline{\mathbf{I}}_{nl}$ are defined as:

$$\overline{\mathbf{I}}_p = \begin{bmatrix} n_{\overline{x}} & 0 & 0 \\ 0 & \frac{a}{b} n_{\overline{y}} & 0 \\ \frac{a}{b} n_{\overline{y}} & n_{\overline{x}} & 0 \end{bmatrix} \qquad \overline{\mathbf{I}}_n = \begin{bmatrix} 0 & 0 & n_{\overline{x}} \\ 0 & 0 & \frac{a}{b} n_{\overline{y}} \\ 0 & 0 & 0 \end{bmatrix} \qquad \overline{\mathbf{I}}_{nl} = \begin{bmatrix} n_{\overline{x}} & 0 & 0 \\ \frac{a}{b} n_{\overline{y}} & 0 & 0 \\ 0 & n_{\overline{x}} & 0 \\ 0 & \frac{a}{b} n_{\overline{y}} & 0 \\ 0 & 0 & n_{\overline{x}} \\ 0 & 0 & \frac{a}{b} n_{\overline{y}} \end{bmatrix} \tag{43}$$

The terms $n_{\overline{x}}$ and $n_{\overline{y}}$ are the components of the normal vector $\overline{\mathbf{n}}$ to the boundary $\overline{\Gamma}$ along the directions $\overline{x}$ and $\overline{y}$, respectively. Invoking the arbitrariness of the virtual variations $\delta \overline{\mathbf{u}}_\tau^k$, the strong form formulation of the problem is derived from Eq. (42). Using matrix notation, it is written as:

$$\begin{cases} \overline{\mathbf{D}}_p^{\mathrm{T}} \overline{\mathbf{R}}_{p\tau}^k + \overline{\mathbf{D}}_n^{\mathrm{T}} \overline{\mathbf{R}}_{n\tau}^k - \overline{\mathbf{R}}_{n\tau_z}^k + \overline{\lambda} \overline{\mathbf{D}}_{nl}^{\mathrm{T}} \overline{\mathbf{\Sigma}}_{0p}^{\mathrm{k}} \overline{\mathbf{D}}_{nl} \overline{\mathbf{u}}_s^k \overline{J}_{\tau s}^k = 0 & \text{on} \quad \overline{\Omega} \\ \overline{\mathbf{I}}_p^{\mathrm{T}} \overline{\mathbf{R}}_{p\tau}^k + \overline{\mathbf{I}}_n^{\mathrm{T}} \overline{\mathbf{R}}_{n\tau}^k + \overline{\lambda} \overline{\mathbf{I}}_{nl}^{\mathrm{T}} \overline{\mathbf{\Sigma}}_{0p}^{\mathrm{k}} \overline{\mathbf{D}}_{nl} \overline{\mathbf{u}}_s^k \overline{J}_{\tau s}^k = 0 \quad \text{or} \quad \delta \overline{\mathbf{u}}_\tau^k = 0 & \text{on} \quad \overline{\Gamma} \end{cases} \tag{44}$$

6.3 Equations in terms of displacements

Under the assumption of linearly elastic material, the governing equations can be expressed in terms of the generalized displacements $\overline{\mathbf{u}}_s^k$. After substitution of Eq. (38) into the stress resultants of Eq. (40), the system of partial differential equations Eq. (44) is re-written as:

$$\begin{cases} \left(\mathcal{L}_{\tau s}^k + \overline{\lambda} \mathcal{G}_{\tau s}^k\right) \overline{\mathbf{u}}_s^k = 0 & \text{on} \quad \overline{\Omega} \\ \left(\mathcal{B}_{\tau s}^k + \overline{\lambda} \mathcal{H}_{\tau s}^k\right) \overline{\mathbf{u}}_s^k = 0 \quad \text{or } \delta \overline{\mathbf{u}}_\tau^k & \text{on} \quad \overline{\Gamma} \end{cases} \tag{45}$$

where the differential operators $\mathcal{L}_{\tau s}^k$ and $\mathcal{G}_{\tau s}^k$ are the 3×3 fundamental nuclei of the formulation relative to the linear and geometric stiffness, respectively. Their expression is given by:

$$\begin{aligned} \mathcal{L}_{\tau s}^k = &\overline{\mathbf{D}}_p^{\mathrm{T}} \overline{\mathbf{C}}_p^k \overline{J}_{\tau s}^k \overline{\mathbf{D}}_p + \overline{\mathbf{D}}_p^{\mathrm{T}} \overline{\mathbf{C}}_{pn}^k \overline{J}_{\tau s}^k \overline{\mathbf{D}}_p + \overline{\mathbf{D}}_p^{\mathrm{T}} \overline{\mathbf{C}}_{pn}^k \overline{J}_{\tau s_z}^k + \overline{\mathbf{D}}_n^{\mathrm{T}} \overline{\mathbf{C}}_{pn}^{k\,\mathrm{T}} \overline{J}_{\tau s}^k \overline{\mathbf{D}}_p + \overline{\mathbf{D}}_n^{\mathrm{T}} \overline{\mathbf{C}}_{nn}^k \overline{J}_{\tau s}^k \overline{\mathbf{D}}_n \\ &+ \overline{\mathbf{D}}_n^{\mathrm{T}} \overline{\mathbf{C}}_{nn}^k \overline{J}_{\tau s_z}^k - \overline{\mathbf{C}}_{pn}^{k\,\mathrm{T}} \overline{J}_{\tau_z s}^k \overline{\mathbf{D}}_p - \overline{\mathbf{C}}_{nn}^k \overline{J}_{\tau_z s}^k \overline{\mathbf{D}}_n - \overline{J}_{\tau_z s_z}^k \overline{\mathbf{C}}_{nn}^k \end{aligned} \tag{46}$$

and:

$$\mathcal{G}^k_{\tau s} = \overline{\mathbf{D}}^{\mathrm{T}}_{nl} \overline{\mathbf{\Sigma}}^k_{0p} \overline{J}^k_{\tau s} \overline{\mathbf{D}}_{nl} \tag{47}$$

where the terms $\overline{J}^k_{\tau s_z}$, $\overline{J}^k_{\tau_z s}$ and $\overline{J}^k_{\tau_z s_z}$ are thickness integrals whose expression is provided in the Appendix. Similarly, the terms $\mathcal{B}^k_{\tau s}$ and $\mathcal{H}^k_{\tau s}$ of Eq. (45) are the fundamental nuclei of the boundary conditions, which are obtained as:

$$\begin{aligned}\mathcal{B}^k_{\tau s} = {} & \overline{\mathbf{I}}^{\mathrm{T}}_p \overline{\mathbf{C}}^k_p \overline{J}^k_{\tau s} \overline{\mathbf{D}}_p + \overline{\mathbf{I}}^{\mathrm{T}}_p \overline{\mathbf{C}}^k_{pn} \overline{J}^k_{\tau s} \overline{\mathbf{D}}_p + \overline{\mathbf{I}}^{\mathrm{T}}_p \overline{\mathbf{C}}^k_{pn} \overline{J}^k_{\tau s_z} + \overline{\mathbf{I}}^{\mathrm{T}}_n \overline{\mathbf{C}}^{k^{\mathrm{T}}}_{pn} \overline{J}^k_{\tau s} \overline{\mathbf{D}}_p + \overline{\mathbf{I}}^{\mathrm{T}}_n \overline{\mathbf{C}}^k_{nn} \overline{J}^k_{\tau s} \overline{\mathbf{D}}_n \\ & + \overline{\mathbf{I}}^{\mathrm{T}}_n \overline{\mathbf{C}}^k_{nn} \overline{J}^k_{\tau s_z} - \overline{\mathbf{C}}^{k^{\mathrm{T}}}_{pn} \overline{J}^k_{\tau_z s} \overline{\mathbf{D}}_p - \overline{\mathbf{C}}^k_{nn} \overline{J}^k_{\tau_z s} \overline{\mathbf{D}}_n - \overline{J}^k_{\tau_z s_z} \overline{\mathbf{C}}^k_{nn}\end{aligned} \tag{48}$$

and:

$$\mathcal{H}^k_{\tau s} = \overline{\mathbf{I}}^{\mathrm{T}}_{nl} \overline{\mathbf{\Sigma}}^k_{0p} \overline{J}^k_{\tau s} \overline{\mathbf{D}}_{nl} \tag{49}$$

It is worth mentioning that the expressions of the fundamental nuclei of Eqs. (46) to (49) are independent on the order of the plate theory, and are formally identical for both EDN and LDN theories.

6.4 Boundary conditions at the simply-supported edges

The two longitudinal edges at $\overline{y} = 0, 1$ are subjected to simply-supported boundary conditions, so $\delta\overline{u}^k_\tau = \delta\overline{w}^k_\tau = 0$. For these two edges, the components of the vector normal to the boundary are $n_{\overline{x}} = 0$ and $n_{\overline{y}} = 1$. Recalling recalling Eqs. (48) and (49) and expanding their components, the three following scalar equations are derived:

$$\begin{cases} \overline{u}^k_\tau = 0 & \text{for} \quad \overline{y} = 0, 1 \\ \overline{J}^k_{\tau s} \left(\overline{C}^k_{12} \overline{u}^k_{s,\overline{x}} + \overline{C}^k_{22} \dfrac{a}{b} \overline{v}^k_{s,\overline{y}} \right) + \overline{J}^k_{\tau s_z} \overline{C}^k_{23} \overline{w}^k_+ \overline{\lambda J}^k_{\tau s} \overline{\sigma}^k_{0\overline{y}\overline{y}} \dfrac{a}{b} \overline{v}^k_{s,\overline{y}} \varphi = 0 & \text{for} \quad \overline{y} = 0, 1 \\ \overline{w}^k_\tau = 0 & \text{for} \quad \overline{y} = 0, 1 \end{cases} \tag{50}$$

The first and the third terms of Eq. (50) are the essential conditions, while the second one is the natural condition regarding the equilibrium along the $\overline{y}$ direction.

6.5 Boundary conditions at the transverse edges

The two parallel transverse edges at $\overline{x} = 0, 1$ can be subjected to any combination of free, simply-supported and clamped boundary conditions. In this case, the components of the normal vector are $n_{\overline{x}} = 0$ and $n_{\overline{y}} = 1$. By expanding Eqs. (48) and (49), the following set of boundary conditions is derived:

$$\begin{cases} \overline{J}^k_{\tau s} \left(\overline{C}^k_{11} \overline{u}^k_{s,\overline{x}} + \dfrac{a}{b} \overline{C}^k_{12} \overline{v}^k_{s,\overline{y}} \right) + \overline{J}^k_{\tau s_z} \overline{C}^k_{13} \overline{w}^k_s + \overline{\lambda J}^k_{\tau s} \overline{\sigma}^k_{0\overline{x}\overline{x}} \overline{u}^k_{s,\overline{x}} \varphi = 0 & \text{or} \quad \delta\overline{u}^k_\tau = 0 \\ \overline{J}^k_{\tau s} \overline{C}^k_{66} \left(\dfrac{a}{b} \overline{u}^k_{s,\overline{y}} + \overline{v}^k_{s,\overline{x}} \right) + \overline{\lambda J}^k_{\tau s} \overline{\sigma}^k_{0\overline{x}\overline{x}} \overline{v}^k_{s,\overline{x}} \varphi = 0 & \text{or} \quad \delta\overline{v}^k_\tau = 0 \\ \overline{J}^k_{\tau s} \overline{C}^k_{55} \overline{w}^k_{s,\overline{x}} + \overline{J}^k_{\tau s_z} \overline{C}^k_{55} \overline{u}^k_s + \overline{\lambda J}^k_{\tau s} \overline{\sigma}^k_{0\overline{x}\overline{x}} \overline{w}^k_{s,\overline{x}} = 0 & \text{or} \quad \delta\overline{w}^k_\tau = 0 \end{cases} \tag{51}$$

In the case of free-edges, the three virtual variations are not null, and the three boundary conditions are those reported in the left part of Eq. (51). When the edges are simply-supported, $\delta\overline{v}^k_\tau = \delta\overline{w}^k_\tau = 0$, whereas in case of clamped edges, all the virtual variations are null.

7 Lévy solution

The system of equations of Eq. (45) can be solved exactly adopting the Lévy-type solution procedure [1]. It consists in reducing the set of partial differential governing equations into a system of ordinary differential equations, whose solution can be sought in exact form.

For a plate with two parallel simply-supported edges at $\overline{y} = 0, 1$, the generalized displacement components $\overline{u}_s^k$, $\overline{v}_s^k$ and $\overline{w}_s^k$ can be expanded by assuming separation of variable, with the following trigonometric series:

$$\begin{aligned} \overline{u}_s^k(\overline{x}, \overline{y}) &= \overline{U}_{sm}^k(\overline{x}) \sin \beta_m \overline{y} \\ \overline{v}_s^k(\overline{x}, \overline{y}) &= \overline{V}_{sm}^k(\overline{x}) \cos \beta_m \overline{y} \\ \overline{w}_s^k(\overline{x}, \overline{y}) &= \overline{W}_{sm}^k(\overline{x}) \sin \beta_m \overline{y} \end{aligned} \tag{52}$$

where the functions $\overline{U}_{sm}^k$, $\overline{V}_{sm}^k$ and $\overline{W}_{sm}^k$ define the $\overline{x}$-wise components of the displacement field of the generic layer k of the laminate, and:

$$\beta_m = m\pi \tag{53}$$

where m is a positive integer defining the number of halfwaves along the direction $\overline{y}$.

It is straightforward to substitute Eq. (52) into Eq. (50) and verify that the expressions of Eq. (52) identically satisfy the boundary conditions of simply-supported edges at $\overline{y} = 0, 1$.

By substitution of Eq. (52) into Eq. (45), the system of ordinary differential equations resulting from application of the Lévy-type approach is derived as:

$$\begin{cases} \left(\mathbf{L}_2^{k\tau s} + \overline{\lambda}\mathbf{L}_{20}^{k\tau s}\right)\overline{\mathbf{U}}_{s,\overline{x}\overline{x}}^k - \mathbf{L}_1^{k\tau s}\overline{\mathbf{U}}_{s,\overline{x}}^k - \left(\mathbf{L}_0^{k\tau s} + \overline{\lambda}\mathbf{L}_{00}^{k\tau s}\right)\overline{\mathbf{U}}_s^k = \mathbf{0} & \text{on} \quad \overline{\Omega} \\ \left(\mathbf{B}_1^{k\tau s} + \overline{\lambda}\mathbf{B}_{10}^{k\tau s}\right)\overline{\mathbf{U}}_{s,\overline{x}}^k + \mathbf{B}_0^{k\tau s}\overline{\mathbf{U}}_s^k = \mathbf{0} & \text{for} \quad \overline{x} = 0, 1 \end{cases} \tag{54}$$

which is a system of second-order ordinary differential equations in the unknowns $\overline{\mathbf{U}}_s^k = \overline{\mathbf{U}}_s^k(\overline{x})$, where:

$$\overline{\mathbf{U}}_s^k = \left\{ \overline{U}_{sm}^k \quad \overline{V}_{sm}^k \quad \overline{W}_{sm}^k \right\}^{\mathrm{T}} \tag{55}$$

The expressions of the matrices $\mathbf{L}^{k\tau s}$ and $\mathbf{B}^{k\tau s}$ are summarized in the Appendix. It is observed that the matrices $\mathbf{B}^{k\tau s}$ are related to the boundary conditions, and their expressions depend on the type of boundary conditions.

7.1 Assembled equations and state-space solution

The system of Eq. (54) defines the equilibrium of the generic ply k, and needs to be assembled to impose the equilibrium at laminate level. The matrices relative to each ply are obtained by expanding the nuclei over the indices τ and s. Then, the equations of the multilayered plate are built-up by assembling the contributions of the various plies. Following the assembly procedure outlined in Refs. [31, 32], the equilibrium equations of the multilayered plate take the form:

$$\begin{cases} \left(\mathbf{L}_2 + \overline{\lambda}\mathbf{L}_{20}\right)\overline{\mathbf{U}}_{,\overline{x}\overline{x}} - \mathbf{L}_1\overline{\mathbf{U}}_{,\overline{x}} - \left(\mathbf{L}_0 + \overline{\lambda}\mathbf{L}_{00}\right)\overline{\mathbf{U}} = \mathbf{0} & \text{on} \quad \overline{\Omega} \\ \left(\mathbf{B}_1 + \overline{\lambda}\mathbf{B}_{10}\right)\overline{\mathbf{U}}_{,\overline{x}} + \mathbf{B}_0\overline{\mathbf{U}} = \mathbf{0} & \text{for} \quad \overline{x} = 0, 1 \end{cases} \tag{56}$$

corresponding to $3(N+1)$ equations and $6(N+1)$ boundary conditions for EDN theories, and $3(N+1)N_l - 3(N_l-1)$ equations and $6(N+1)N_l - 6(N_l-1)$ boundary conditions for LDN theories.

The exact solution of Eq. (56) is obtained referring to the state-space approach. In particular, the system of Eq. (56) is transformed into a system of first-order differential equations by introducing the state $\mathbf{Z}$, defined as:

$$\mathbf{Z}(\overline{x}) = \left\{ \overline{\mathbf{U}}_{,\overline{x}} \quad \overline{\mathbf{U}} \right\}^{\mathrm{T}} \tag{57}$$

From Eq. (57), the second-order system of Eq. (56) becomes:

$$\begin{cases} \mathbf{Z}(\overline{x})_{,\overline{x}} = \mathbf{A}\mathbf{Z}(\overline{x}) & \text{on} \quad \overline{\Omega} \\ \mathbf{B}\mathbf{Z}(\overline{x}) = \mathbf{0} & \text{for} \quad \overline{x} = 0, 1 \end{cases} \tag{58}$$

where:

$$\mathbf{A} = \begin{bmatrix} \mathbf{L}_2 + \overline{\lambda}\mathbf{L}_{20} & \mathbf{0} \\ \mathbf{0} & \mathbf{I} \end{bmatrix}^{-1} \begin{bmatrix} \mathbf{L}_1 & \mathbf{L}_0 + \overline{\lambda}\mathbf{L}_{00} \\ \mathbf{I} & \mathbf{0} \end{bmatrix} \tag{59}$$

$$\mathbf{B} = \begin{bmatrix} \mathbf{B}_1 + \lambda\mathbf{B}_{10} & \mathbf{B}_0 \end{bmatrix} \tag{60}$$

The general solution of Eq. (58) is:

$$\mathbf{Z}(\overline{x}) = e^{\mathbf{A}\overline{x}}\mathbf{c} \tag{61}$$

where $\mathbf{c}$ is a vector of constants related to the boundary conditions of the problem. After computing the spectral decomposition of the matrix $\mathbf{A}$, Eq. (61) can be re-written as:

$$\mathbf{Z}(\overline{x}) = \mathbf{V}\mathrm{diag}\left(e^{\lambda_i \overline{x}}\right)\mathbf{V}^{-1}\mathbf{c} \tag{62}$$

where $\mathbf{V}$ and λ_i are the eigenvector matrix and the corresponding eigenvalues of $\mathbf{A}$, respectively.

The boundary conditions of Eq. (58) are finally imposed as:

$$\mathbf{H}(\overline{x})\,\mathbf{c} = \mathbf{0} \qquad \text{for} \qquad \overline{x} = 0, 1 \tag{63}$$

where:

$$\mathbf{H}(\overline{x}) = \mathbf{B}\mathbf{V}\mathrm{diag}\left(e^{\lambda_i \overline{x}}\right)\mathbf{V}^{-1}\mathbf{c} \tag{64}$$

The bifurcation load associated to a given number of halfwaves m is found by computing the smallest value of λ_i for which the determinant of $\mathbf{H}$ vanishes. The buckling load is obtained as the lowest among all the possible values obtained for different integer values of m.

8 Results

The results obtained with the variable-kinematic plate theory and the Lévy-type solution procedure are here presented. Composite plates are studied under the assumption of two parallel edges simply-supported at $y = 0, b$, and two parallel edges subjected to any combination of boundary conditions at $x = 0, a$. The letters F, S and C are used to denote free, simply-supported and clamped edges, respectively. Both loading

conditions of uniaxial and biaxial compression are discussed.

Firstly, comparisons are presented with exact 2D and 3D solutions existing in the literature to validate the proposed approach. Then, a wide set of results relative to the biaxial buckling of cross-ply plates with various boundary condition is reported and proposed as a benchmark for future investigations.

The material properties considered in the examples are:

- Material 1: see Eq. (65)
- Material 2: E_1/E_2 variable, $G_{12}/E_2 = G_{13}/E_2 = 0.6$, $G_{23}/E_2 = 0.5$, $\nu_{12} = \nu_{13} = \nu_{23} = 0.25$
- Material 3: E_1/E_2 variable, $G_{12}/E_2 = G_{13}/E_2 = 0.5$, $G_{23}/E_2 = 0.2$, $\nu_{12} = \nu_{13} = \nu_{23} = 0.25$

The elastic properties of Material 1 are those of the aragonite crystals, and are taken form the works of Bisplinghoff and Mar [33] and Srinivas and Rao [22]. The properties are reported in terms of the elastic constants C_{ik}, and, for convenience, are here summarized:

$$\begin{bmatrix} C_{11} & C_{12} & 0 & 0 & 0 & C_{13} \\ C_{12} & C_{22} & 0 & 0 & 0 & C_{23} \\ 0 & 0 & C_{66} & 0 & 0 & 0 \\ 0 & 0 & 0 & C_{55} & 0 & 0 \\ 0 & 0 & 0 & 0 & C_{44} & 0 \\ C_{13} & C_{23} & 0 & 0 & 0 & C_{33} \end{bmatrix} = C_{11} \begin{bmatrix} 1.000000 & 0.233190 & 0 & 0 & 0 & 0.010776 \\ 0.233190 & 0.543103 & 0 & 0 & 0 & 0.098276 \\ 0 & 0 & 0.262931 & 0 & 0 & 0 \\ 0 & 0 & 0 & 0.159914 & 0 & 0 \\ 0 & 0 & 0 & 0 & 0.266810 & 0 \\ 0.010776 & 0.098276 & 0 & 0 & 0 & 0.530172 \end{bmatrix} \tag{65}$$

The dimensional form of Eq. (65) is obtained by taking $C_{11} = 159.9584$ GPa.

8.1 Comparison with literature

Uniaxial compression

A first comparison is performed with the results of Srinivas and Rao [22], and deals with the buckling analysis of a square composite plate composed of one layer of Material 1. The panel is simply-supported along the four edges and is subjected to loading conditions of pure compression applied with an imposed stress P_x at the edges at $x = 0$, a. As far as the plate is made of a single layer, no distinction exists between the load introduction by means of an imposed axial stress or strain, meaning that $N_x^\sigma = N_x^\epsilon = N_x^\varepsilon$.

The results are reported in Table 1 in terms of the parameter $k_x^\sigma = \dfrac{12}{\pi^2}\dfrac{N_x^\sigma}{E_1}\left(\dfrac{b}{h}\right)^2$. The nondimensional buckling loads obtained with the present method are verified against those obtained by Srinivas and Rao using exact 3D elasticity solutions. The comparison is performed for plate theories ED2, ED4, LD2 and LD4. Furthermore, the results are presented by considering the nonlinear terms according to von Kármán approximation, denoted in the table as vK, or keeping the full expression, denoted in the table as Full. A variable range of width-to-thickness ratios is investigated, from $b/h = 20$, corresponding to a moderately thick configuration, until $b/h = 5$, corresponding to a thick plate. The percent differences are reported in the parenthesis and are calculated taking the solution of Ref. [22] as a reference.

As observed from Table 1, no difference is observed between theories of corresponding order, i.e. ED2 and LD2, and ED4 and LD4. Indeed, the equivalent displacement and the layerwise theories are formally identical when the plate is composed of one single layer. The comparison of the results with the exact 3D

solution highlights two main aspects. Firstly, the distinction between the results obtained with second- and fourth-order theories is not particularly relevant if the ratio b/h is equal to 20. On the other hand, relatively high errors are obtained using a second-order theory for plates with b/h equal to 5. A similar consideration holds for the expression of the strain tensor. The von Kármán approximation is appropriate for moderately thick plates, but the quality of results decreases as the width-to-thickness ratio is reduced. For b/h equal to 5, the difference between the 3D results and the LD4 with von Kármán approximation is approximately 4%. The accuracy of the present method is demonstrated by the exact predictions achieved using LD4 and ED4 theories in conjunction with the full strain tensor expression, which lead to the same results obtained by Srinivas and Rao [22].

The second comparison regards the buckling analysis of a square three-ply plate. The elastic properties of the mid-ply are those of Eq. (65), while those of the top and bottom plies are obtained by scaling the values of Eq. (65) with the factor β of Table 2. The relative ply thicknesses are $h_1/h = 0.1$, $h_2/h = 0.8$, where h_1 and h_2 are the thicknesses of the outer and middle plies, respectively. The width-to-thickness ratio is $b/h = 10$. The panel is simply-supported along the four edges and is loaded with an imposed uniform strain. The stress acting on each ply is proportional to its stiffness and, due to the definition of the material elastic properties, $N_x^\epsilon = N_x^\varepsilon$.

The results are presented in terms of the nondimensional buckling load $k_x^\varepsilon = \frac{12}{\pi^2}\frac{\sigma_x^k}{C_{11}^k}\left(\frac{b}{h}\right)^2$ and percent differences are reported in the parenthesis with respect to the exact three-dimensional solution.

Due to the presence of three plies, EDN and LDN theories lead to different results. While good accuracy is observed for layerwise theories, even in the case of LD2, the errors obtained using EDN theory can be as high as 36%. The discrepancy between the buckling loads obtained with LDN and EDN theories is exacerbated by high values of β, corresponding to high stiffness discontinuities between the mid-ply and the outer ones. On the other hand, the results computed with and without von Kármán approximation are almost insensitive to the orthotropy ratio β. It is worth noting that a percent error beyond 4% is achieved for $\beta = 4$ with ED4 theory, even adopting the full expression of the strain tensor. This example well illustrates the inadequacy of EDN theories in presence of large stiffness variations along the thickness direction. On the contrary, excellent results are guaranteed by LD4 theory along with full expression of the strain tensor. These results are in close agreement with the exact 3D solutions of Ref. [22].

Another comparison is performed with the results computed by Noor [23] using 3D elasticity solution. Only LD4 theory is now applied.

A square panel, composed of a variable number of layers of Material 2, is considered. The orthotropy ratio E_1/E_2 varies between 3 and 40, and the width-to-thickness ratio is fixed to 10.

The plate is simply-supported at the four edges, and is loaded with an imposed axial strain. The pre-buckling condition is characterized by a stress distribution proportional to the stiffness of the layers, but deformation compatibility between the layers is not ensured, as the assumption of equal Poisson's ratios is invoked [23]. Therefore, the thickness resultant of the axial stress is here denoted as N_x^ϵ. Symmetric and unsymmetric cross-ply laminates, with a total number N_l of layers, are considered. The plies are stacked, alternately, at

0° and 90° and, for symmetric laminates, the 0° plies are those in the outer positions. The total thickness of the plies at 0° and 90° is the same. In case of symmetric lay-ups, the thickness of the plies at 90° is:

$$h_{90} = h_0 \frac{N_l + 1}{N_l - 1} \tag{66}$$

where h_{90} and h_0 are the thicknesses of the plies at 90° and 0°, respectively.

The comparison of the results is illustrated in Table 3 in terms of the nondimensional buckling load $k_x^\epsilon = \frac{N_x^\epsilon b^2}{E_2 h^3}$. As observed, close agreement is obtained between exact 3D and LD4 solutions with full expression of the nonlinear strain tensor. More specifically, the results are identical in the case of unsymmetric lay-ups, while a slight difference is observed for symmetric lay-ups. In any case, the maximum deviation with respect to the 3D solution is below 0.01%. The error due to the von Kármán approximation is below 2.31%, and is almost independent on the orthotropy ratio as well as the number of plies.

Biaxial compression

A comprehensive set of solutions for buckling loads under biaxial compression and various boundary conditions is reported in the work of Xiang et al. [8], where exact results are obtained using the Lévy-type procedure in conjunction with first-order shear deformation theory. Square composite plates with a variable number of layers of Material 2 are considered. The orthotropy ratio E_1/E_2 is fixed to 40, while the plies are stacked by alternating layers at 0° and 90°. As opposed to the previous example, each ply has the same thickness. The plates are simply-supported along the parallel edges at $y = 0, b$, and subjected to various boundary conditions along the two other edges. Biaxial compression is applied with a ratio $N_x^\varepsilon/N_y^\varepsilon = 1$, where deformation compatibility is assumed as far as the theory of Ref. [8] is based on FSDT.

The nondimensional buckling loads $k_x^\varepsilon = \frac{N_x^\varepsilon}{b^2/E_2 h^3}$ are reported in Tables 4, 5 and 6 with regard to FF, FS and FC boundary conditions for different aspect ratios and thickness-to-width ratios. Overall, good agreement is achieved for b/h equal to 20 between the results obtained with LD4 and those derived by Xiang et al. [8]. In this case, the maximum difference is approximately 1%. The discrepancies rise to approximately 6% for b/h equal to 10, and become greater than 10% for b/h equal to 6.67. This conclusion holds for all the three different set of boundary conditions. The inadequacy of the first-order theory for moderately thick plates is then highlighted. Regarding the expression of the strain tensor, the error introduced by the von Kármán approximation depends on the width-to-thickness ratio, with percent differences below 0.5% for $b/h = 20$, around 1% for $b/h = 10$ and beyond 1% for $b/h = 6.67$. On the other hand, no significant dependence is observed on the orthotropy ratio and the boundary conditions. Lévy-type solutions are derived by Thai and Kim [21] using two variable refined plate theory for orthotropic plates under biaxial compression. The plates are characterized by one single layer of Material 3. They are subjected to various boundary conditions, and are loaded in biaxial compression with $N_x^\varepsilon = N_y^\varepsilon = 1$. The plate theory used by Thai and Kim determines a pre-buckling stress state which intrinsically guarantees deformation compatibility. Thus, results are reported in Table 7 in terms of the nondimensional buckling load $k_x^\varepsilon = \frac{N_x^\varepsilon a^2}{E_2 h^3}$. The comparison is presented with the results obtained with LD4 theory and full expression of the strain tensor.

Two distinct approaches are adopted in Table 7 to compute the buckling load. In a first case, the number of halfwaves m is fixed to 1 and the corresponding bifurcation load is reported. In the second case, the number of halfwaves is varied between 1 and sufficiently large integer, and the buckling load is obtained as the minimum between all the computed bifurcation loads. This second approach allows to obtain the first buckling load. In Table 7, the number of halfwaves is reported in the superscript.

Although not stated in Ref. [21], the authors assume that the loads reported by Thai and Kim are computed by restricting the buckling mode to exhibit one single halfwave along the y-direction. Indeed, despite some differences related to the use of different theories, substantial agreement is observed between the results obtained with the two theories if $m = 1$ is assumed. As expected, the buckling loads obtained with the theory of Ref. [21] are higher. Increasing differences are observed as the thickness-to-length ratio a/h is reduced and the material orthotropy ratio of the material is increased. When $a/h = 5$, the maximum difference between LD4 and two variable refined theory, even assuming $m = 1$, is 40%.

8.2 Benchmark results

Having demonstrated the accuracy of the buckling loads obtained with the present method, a set of benchmark results is now proposed using LD4 theory with full expression of the strain tensor. The scarcity of high-accuracy solutions for the biaxial buckling of cross-ply plates suggests the use of these results as a benchmark for future investigations by other researchers. To cover a wide set of configurations, buckling loads are computed for cross-ply plates subjected to various boundary and loading conditions. Furthermore, different ratios of material orthotropy, thickness-to-width and plate dimensions are investigated.

The plates are composed of three layers of Material 2, oriented at $[0^\circ/90^\circ/0^\circ]$. The total thickness of the plies at 0° and 90° is the same, meaning that relation between the thickness of the plies at 90° and 0° is given by Eq. (66). The pre-buckling stress is determined using two approaches. Firstly, an imposed stress is assumed, equal for all the plies. In this case, the stress resultants are denoted as N_x^σ and N_y^σ. In a second case, an imposed compatible strain is postulated, and the corresponding stress distribution is computed following the approach outlined in Section 4.3. Strain compatibility is ensured, and the corresponding stress resultants are N_x^ε and N_y^ε. This second set of solutions can be particularly useful when validating newly developed finite elements, where pre-buckling conditions are computed from the solution of a linear static problem and, intrinsically, satisfy compatibility condition between the layers.

The results are reported in Tables 8 and 9 for load ratios N_x/N_y equal to 1 and 2, respectively. In both cases, the number of halfwaves along the y direction is reported in the superscript. As observed, the difference between the results obtained with the two pre-buckling calculations strategy are small, although not null.

9 Conclusions

A variable-kinematic formulation has been presented for the exact solution of the buckling equations of biaxially loaded cross-ply plates. Solutions can be derived for various boundary conditions on the basis of

the Lévy-type approach. The main advantage of the proposed formulation regards its invariance on the kinematic-assumptions, which allows to consider low-order as well as higher-order theories within the same framework. Furthermore, it automatically accounts for two distinct class of theories, layerwise and equivalent layer.

The results have been validated against exact 3D solutions available in the literature, both for uniaxial and biaxial compression loads. It was demonstrated that the results obtained with LD4 theory, in conjunction with the full expression of the nonlinear strain tensor, are almost identical to 3D solutions. The same conclusion was achieved for ED4 theory, provided the plate is not characterized by abrupt stiffness variations along the thickness. In this latest case, the accuracy of ED4 results decreases as the differential stiffness of the layers becomes more pronounced.

The influence of von Kármán approximation was investigated. It was found that its effect is almost negligible for thin plates, while it determines an increasing loss of accuracy as the panel gets thicker. On the other hand, the approximation is not significantly influenced by the material orthotropy ratio, boundary conditions and number of layers.

Finally, the high level of accuracy of LD4 results suggested to compute a wide set of biaxial buckling loads which can be a useful reference for future studies to validate numerical and analytical tools.

References

[1] J.N. Reddy. *Mechanics of Laminated Composite Plates and Shells: Theory and Analysis*. CRC Press, Boca Raton, 2004.

[2] P. Qiao and L. Shan. Explicit local buckling analysis and design of fiber-reinforced plastic composite structural shapes. *Composite Structures*, 70(4):468–483, 2005.

[3] C. Bisagni and R. Vescovini. Analytical formulation for local buckling and post-buckling analysis of stiffened laminated panels. *Thin-Walled Structures*, 47(3):318–334, 2009.

[4] R. Vescovini and C. Bisagni. Single-mode solution for post-buckling analysis of composite panels with elastic restraints loaded in compression. *Composites Part B: Engineering*, 43(3):1258–1274, 2012.

[5] K.M. Liew, Y. Xiang, and S. Kitipornchai. Navier's solution for laminated plate buckling with pre-buckling in-plane deformation. *International Journal of Solids and Structures*, 33(13):1921–1937, 1996.

[6] K.M. Liew, Y. Xiang, and S. Kitipornchai. Analytical buckling solutions for Mindlin plates involving free edges. *International Journal of Mechanical Sciences*, 38(10):1127–1138, 1996.

[7] R.F. Palardy and A.N. Palazotto. Buckling and vibration of composite plates using the Levy method. *Composite Structures*, 14(1):61–86, 1990.

[8] Y. Xiang, K.M. Liew, and S. Kitipornchai. Exact buckling solutions for composite laminates: proper free edge conditions under in-plane loadings. *Acta Mechanica*, 117(1-4):115–128, 1996.

[9] A.M. Zenkour. Buckling and free vibration of elastic plates using simple and mixed shear deformation theories. *Acta Mechanica*, 146(3-4):183–197, 2001.

[10] J.N. Reddy and N.D. Phan. Stability and vibration of isotropic, orthotropic and laminated plates according to a higher-order shear deformation theory. *Journal of Sound and Vibration*, 98(2):157–170, 1985.

[11] J. Hadian and A.H. Nayfeh. Free vibration and buckling of shear-deformable cross-ply laminated plates using the state-space concept. *Computers & Structures*, 48(4):677–693, 1993.

[12] A.A. Khdeir. Free vibration and buckling of symmetric cross-ply laminated plates by an exact method. *Journal of Sound and Vibration*, 126(3):447–461, 1988.

[13] A.A. Khdeir and L. Librescu. Analysis of symmetric cross-ply laminated elastic plates using a higher-order theory: Part II-buckling and free vibration. *Composite Structures*, 9(4):259–277, 1988.

[14] A.A. Khdeir. Free vibration and buckling of unsymmetric cross-ply laminated plates using a refined theory. *Journal of Sound and Vibration*, 128(3):377–395, 1989.

[15] I. Shufrin and M. Eisenberger. Stability and vibration of shear deformable plates - first order and higher order analyses. *International Journal of Solids and Structures*, 42(3):1225–1251, 2005.

[16] A.J.M. Ferreira, C.M.C Roque, A.M.A Neves, R.M.N Jorge, C.M Mota Soares, and J.N. Reddy. Buckling analysis of isotropic and laminated plates by radial basis functions according to a higher-order shear deformation theory. *Thin-Walled Structures*, 49(7):804–811, 2011.

[17] H. Matsunaga. Free vibration and stability of thick elastic plates subjected to in-plane forces. *International Journal of Solids and Structures*, 31(22):3113–3124, 1994.

[18] H. Matsunaga. Buckling instabilities of thick elastic plates subjected to in-plane stresses. *Computers & Structures*, 62(1):205–215, 1997.

[19] R.P. Shimpi. Refined plate theory and its variants. *AIAA Journal*, 40(1):137–146, 2002.

[20] S.E. Kim, H.T. Thai, and J. Lee. Buckling analysis of plates using the two variable refined plate theory. *Thin-Walled Structures*, 47(4):455–462, 2009.

[21] H.T. Thai and S.E. Kim. Levy-type solution for buckling analysis of orthotropic plates based on two variable refined plate theory. *Composite Structures*, 93(7):1738–1746, 2011.

[22] S. Srinivas and A.K. Rao. Bending, vibration and buckling of simply supported thick orthotropic rectangular plates and laminates. *International Journal of Solids and Structures*, 6(11):1463–1481, 1970.

[23] A.K. Noor. Stability of multilayered composite plates. *Fibre Science and Technology*, 8(2):81–89, 1975.

[24] W.H. Wittrick. Analytical, three-dimensional elasticity solutions to some plate problems, and some observations on Mindlin's plate theory. *International Journal of Solids and Structures*, 23(4):441–464, 1987.

[25] H. Gu and A. Chattopadhyay. Three-dimensional elasticity solution for buckling of composite laminates. *Composite Structures*, 50(1):29–35, 2000.

[26] E. Carrera. A class of two-dimensional theories for anisotropic multilayered plates analysis. *Atti Accademia delle Scienze di Torino. Memorie Scienze Fisiche*, 19:1–39, 1995.

[27] E. Carrera. Theories and finite elements for multilayered, anisotropic, composite plates and shells. *Archives of Computational Methods in Engineering*, 9(2):87–140, 2002.

[28] M. D'Ottavio and E. Carrera. Variable-kinematics approach for linearized buckling analysis of laminated plates and shells. *AIAA Journal*, 48(9):1987–1996, 2010.

[29] F.A. Fazzolari and E. Carrera. Advanced variable kinematics Ritz and Galerkin formulations for accurate buckling and vibration analysis of anisotropic laminated composite plates. *Composite Structures*, 94(1):50–67, 2011.

[30] P. Nali, E. Carrera, and S. Lecca. Assessments of refined theories for buckling analysis of laminated plates. *Composite Structures*, 93(2):456–464, 2011.

[31] L. Dozio. Exact vibration solutions for cross-ply laminated plates with two opposite edges simply supported using refined theories of variable order. *Journal of Sound and Vibration*, 333(8):2347–2359, 2014.

[32] L. Dozio. Exact free vibration analysis of Lévy FGM plates with higher-order shear and normal deformation theories. *Composite Structures*, 111:415–425, 2014.

[33] R. Bisplinghoff and J.W. Mar. *Statics of Deformable Solids*. Courier Dover Publications, 2002.

10 Appendix

Thickness integrals

$$\begin{aligned} \overline{J}^k_{\tau s} &= \int_{-1}^{1} F_\tau F_s \frac{\widehat{h}}{h} d\overline{z} \qquad \overline{J}^k_{\tau s_z} = \int_{-1}^{1} 2F_\tau F_{s,\overline{z}} \frac{a}{h} d\overline{z} \\ \overline{J}^k_{\tau_z s} &= \int_{-1}^{1} 2F_{\tau,\overline{z}} F_s \frac{a}{h} d\overline{z} \quad \overline{J}^k_{\tau_z s_z} = \int_{-1}^{1} 4F_{\tau,\overline{z}} F_{s,\overline{z}} \frac{a^2}{h\widehat{h}} d\overline{z} \end{aligned} \tag{67}$$

Ply level matrices

$$\mathbf{L}_2^{k\tau s} = \overline{J}^k_{\tau s} \begin{bmatrix} \overline{C}^k_{11} & 0 & 0 \\ 0 & \overline{C}^k_{66} & 0 \\ 0 & 0 & \overline{C}^k_{55} \end{bmatrix} \qquad \mathbf{L}_{20}^{k\tau s} = \overline{J}^k_{\tau s} \overline{\sigma}^k_{0\overline{xx}} \begin{bmatrix} \varphi & 0 & 0 \\ 0 & \varphi & 0 \\ 0 & 0 & 1 \end{bmatrix} \tag{68}$$

$$\mathbf{L}_1^{k\tau s} = \begin{bmatrix} 0 & l_{12} & l_{13} \\ -l_{12} & 0 & 0 \\ -l_{13} & 0 & 0 \end{bmatrix} \tag{69}$$

$$\mathbf{L}_0^{k\tau s} = \begin{bmatrix} l_{11} & 0 & 0 \\ 0 & l_{22} & l_{23} \\ 0 & l_{23} & l_{33} \end{bmatrix} \qquad \mathbf{L}_{00}^{k\tau s} = \overline{J}^k_{\tau s} \overline{\sigma}^k_{0\overline{yy}} \beta^2 \begin{bmatrix} \varphi & 0 & 0 \\ 0 & \varphi & 0 \\ 0 & 0 & 1 \end{bmatrix} \tag{70}$$

where:

$$l_{11} = \overline{J}^k_{\tau s} \left(\frac{a}{b}\right)^2 \overline{C}^k_{66} \beta_m^2 + \overline{J}^k_{\tau_z s_z} \overline{C}^k_{55} \tag{71}$$

$$l_{12} = \overline{J}^k_{\tau s} \frac{a}{b} \left(\overline{C}^k_{12} + \overline{C}^k_{66}\right) \beta_m \tag{72}$$

$$l_{13} = \overline{J}^k_{\tau_z s} \overline{C}^k_{55} - \overline{J}^k_{\tau s_z} \overline{C}^k_{13} \tag{73}$$

$$l_{22} = \overline{J}^k_{\tau s} \left(\frac{a}{b}\right)^2 \overline{C}^k_{22} \beta_m^2 + \overline{J}^k_{\tau_z s_z} \overline{C}^k_{44} \tag{74}$$

$$l_{23} = \frac{a}{b} \left(\overline{J}^k_{\tau_z s} \overline{C}^k_{44} - \overline{J}^k_{\tau s_z} \overline{C}^k_{23}\right) \beta_m \tag{75}$$

$$l_{33} = \overline{J}^k_{\tau s} \left(\frac{a}{b}\right)^2 \overline{C}^k_{44} \beta_m^2 + \overline{J}^k_{\tau_z s_z} \overline{C}^k_{33} \tag{76}$$

- free-edge boundary conditions:

$$\mathbf{B}_1^{k\tau s} = \overline{J}^k_{\tau s} \begin{bmatrix} \overline{C}^k_{11} & 0 & 0 \\ 0 & \overline{C}^k_{66} & 0 \\ 0 & 0 & \overline{C}^k_{55} \end{bmatrix} \quad \mathbf{B}_{10}^{k\tau s} = \overline{J}^k_{\tau s} \overline{\sigma}^k_{0\overline{xx}} \begin{bmatrix} \varphi & 0 & 0 \\ 0 & \varphi & 0 \\ 0 & 0 & 1 \end{bmatrix} \quad \mathbf{B}_0^{k\tau s} = \begin{bmatrix} 0 & -\beta_m \overline{C}^k_{12} \overline{J}^k_{\tau s} & \overline{C}^k_{13} \overline{J}^k_{\tau s_z} \\ \beta_m \overline{C}^k_{66} \overline{J}^k_{\tau s} & 0 & 0 \\ \overline{C}^k_{55} \overline{J}^k_{\tau s_z} & 0 & 0 \end{bmatrix} \tag{77}$$

- simply-supported boundary conditions:

$$\mathbf{B}_1^{k\tau s} = \overline{J}_{\tau s}^k \begin{bmatrix} \overline{C}_{11}^k & 0 & 0 \\ 0 & 0 & 0 \\ 0 & 0 & 0 \end{bmatrix} \quad \mathbf{B}_{10}^{k\tau s} = \overline{J}_{\tau s}^k \overline{\sigma}_{0\overline{xx}}^k \begin{bmatrix} \varphi & 0 & 0 \\ 0 & 0 & 0 \\ 0 & 0 & 0 \end{bmatrix} \quad \mathbf{B}_0^{k\tau s} = \begin{bmatrix} 0 & -\beta_m \overline{C}_{12}^k \overline{J}_{\tau s}^k & \overline{C}_{13}^k \overline{J}_{\tau s_z}^k \\ 0 & \delta_{\tau s} & 0 \\ 0 & 0 & \delta_{\tau s} \end{bmatrix} \tag{78}$$

where $\delta_{\tau s}$ is the Kronecker's delta.

- clamped boundary conditions:

$$\mathbf{B}_1^{k\tau s} = \mathbf{B}_{10}^{k\tau s} = \mathbf{0} \quad \mathbf{B}_0^{k\tau s} = \begin{bmatrix} \delta_{\tau s} & 0 & 0 \\ 0 & \delta_{\tau s} & 0 \\ 0 & 0 & \delta_{\tau s} \end{bmatrix} \tag{79}$$

Table 1: Comparison of buckling factor $k_x^\sigma = \dfrac{12}{\pi^2}\dfrac{N_x^\sigma}{E_1}\left(\dfrac{b}{h}\right)^2$ with the exact 3D solutions of Ref. [22] for SS square homogeneous plate of Material 1 loaded in compression. Percent differences are reported in the parenthesis.

	b/h		
	5	10	20
Exact 3D ([22])	2.210	2.770	2.966
ED2 - vK	2.3881 (8.06)	2.8434 (2.65)	2.9874 (0.72)
LD2 - vK	2.3881 (8.06)	2.8434 (2.65)	2.9874 (0.72)
ED4 - vK	2.2977 (3.97)	2.8094 (1.42)	2.9778 (0.40)
LD4 - vK	2.2977 (3.97)	2.8094 (1.42)	2.9778 (0.40)
ED2 - Full	2.2905 (3.64)	2.8027 (1.18)	2.9755 (0.32)
LD2 - Full	2.2905 (3.64)	2.8027 (1.18)	2.9755 (0.32)
ED4 - Full	2.2099 (0.00)	2.7700 (0.00)	2.9660 (0.00)
LD4 - Full	2.2099 (0.00)	2.7700 (0.00)	2.9660 (0.00)

Table 2: Comparison of buckling factor $k_x^{\varepsilon} = \dfrac{12}{\pi^2}\dfrac{\sigma_x^k}{C_{11}^k}\left(\dfrac{b}{h}\right)^2$ with the exact 3D solutions of Ref. [22] for three-ply SS square plate of Material 1 with $b/h = 10$, loaded in compression with an imposed axial strain. Percent differences are reported in the parenthesis.

	$\beta = C_{11}/C_{22}$				
	1	2	5	10	15
Exact 3D ([22])	2.770	3.330	4.046	4.200	4.037
ED2 - vK	2.8437 (2.66)	3.4728 (4.29)	4.4801 (10.73)	5.1701 (23.10)	5.4887 (35.96)
LD2 - vK	2.8206 (1.83)	3.3946 (1.94)	4.1280 (2.03)	4.2782 (1.86)	4.1025 (1.62)
ED4 - vK	2.8096 (1.43)	3.3889 (1.77)	4.1565 (2.73)	4.3835 (4.37)	4.2861 (6.17)
LD4 - vK	2.8096 (1.43)	3.3860 (1.68)	4.1232 (1.91)	4.2758 (1.80)	4.1012 (1.59)
ED2 - Full	2.8029 (1.19)	3.4129 (2.49)	4.3830 (8.33)	5.0429 (20.07)	5.3465 (32.44)
LD2 - Full	2.7808 (0.39)	3.3385 (0.26)	4.0507 (0.12)	4.2028 (0.07)	4.0385 (0.04)
ED4 - Full	2.7703 (0.01)	3.3331 (0.09)	4.0777 (0.78)	4.3030 (2.45)	4.2140 (4.38)
LD4 - Full	2.7703 (0.01)	3.3303 (0.01)	4.0462 (0.00)	4.2006 (0.01)	4.0372 (0.00)

Table 3: Comparison of buckling factor $k_x^\epsilon = \dfrac{N_x^\epsilon b^2}{E_2 h^3}$ with the exact 3D solutions of Ref. [23] for square SS plates of Material 2 with $b/h = 10$ loaded in compression with an imposed axial strain.

Method		Exact 3D ([23])			LD4 - vK			LD4 - Full		
		E_1/E_2			E_1/E_2			E_1/E_2		
Lamination	N_l	3	20	40	3	20	40	3	20	40
Unsymmetric	2	4.6948	7.8196	10.8167	4.7820	7.9998	11.0596	4.6948	7.8196	10.8167
	4	5.1738	13.7429	21.2796	5.2544	13.9331	21.5232	5.1738	13.7429	21.2797
	6	5.2673	15.0014	23.6689	5.3465	15.1862	23.8994	5.2673	15.0014	23.6690
	10	5.3159	15.6685	24.9636	5.3942	15.8498	25.1864	5.3159	15.6685	24.9636
Symmetric	3	5.3044	15.0191	22.8807	5.4109	15.3127	23.2583	5.3051	15.0196	22.8811
	5	5.3255	15.6527	24.5929	5.4196	15.9011	24.9075	5.3258	15.6531	24.5931
	9	5.3352	15.9153	25.3436	5.4220	16.1333	25.6159	5.3354	15.9155	25.3437

Table 4: Comparison of buckling factor $k_x^{\varepsilon} = \dfrac{N_x^{\varepsilon} b^2}{E_2 h^3}$ with the exact FSDT solutions of Ref. [8] for FF plates of Material 2 with $E_1/E_2 = 40$ subjected to biaxial compression with $\dfrac{N_x^{\varepsilon}}{N_y^{\varepsilon}} = 1$.

		FSDT ([8])			LD4-vK			LD4 - Full		
		h/b			h/b			h/b		
N_l	a/b	6.67	10	20	6.67	10	20	6.67	10	20
3	0.5	1.4899	1.6761	1.8462	1.4805	1.6715	1.8459	1.4598	1.6582	1.8414
	1.0	1.6941	1.8268	1.9301	1.6554	1.8061	1.9246	1.6350	1.7945	1.9211
	1.5	1.7607	1.8761	1.9590	1.7017	1.8449	1.9504	1.6859	1.8362	1.9478
	2.0	1.7888	1.8971	1.9717	1.7177	1.8597	1.9614	1.7053	1.8529	1.9594
	2.5	1.8025	1.9073	1.9780	1.7242	1.8663	1.9667	1.7141	1.8607	1.9651
	3.0	1.8100	1.9129	1.9816	1.7272	1.8696	1.9697	1.7186	1.8648	1.9683
5	0.5	1.9132	2.3162	2.6920	1.8129	2.2373	2.6626	1.7842	2.2172	2.6549
	1.0	3.1502	3.7449	4.2398	2.8650	3.5442	4.1702	2.8274	3.5176	4.1605
	1.5	3.9623	4.6971	5.2921	3.5498	4.4130	5.1951	3.5130	4.3864	5.1853
	2.0	4.4346	5.2505	5.9052	3.9482	4.9185	5.7926	3.9142	4.8933	5.7832
	2.5	4.7087	5.5710	6.2603	4.1812	5.2127	6.1392	4.1495	5.1887	6.1301
	3.0	4.8130	5.6295	6.2832	4.3208	5.3542	6.1896	4.2905	5.3202	6.1770
7	0.5	2.0635	2.5757	3.0739	1.9773	2.5053	3.0465	1.9446	2.4819	3.0373
	1.0	3.6482	4.5102	5.2756	3.4108	4.3343	5.2118	3.3648	4.3004	5.1987
	1.5	4.7024	5.8101	6.7745	4.3638	5.5636	6.6861	4.3165	5.5276	6.6721
	2.0	5.3083	6.5558	7.6342	4.9153	6.2712	7.5328	4.8697	6.2355	7.5187
	2.5	5.5633	6.7128	7.6978	5.2259	6.5083	7.6244	5.1812	6.4597	7.6055
	3.0	5.4466	6.6046	7.6022	5.1225	6.3699	7.5182	5.0666	6.3264	7.5013

Table 5: Comparison of buckling factor $k_x^{\varepsilon} = \dfrac{N_x^{\varepsilon} b^2}{E_2 h^3}$ with the exact FSDT solutions of Ref. [8] for FS plates of Material 2 with $E_1/E_2 = 40$ subjected to biaxial compression with $\dfrac{N_x^{\varepsilon}}{N_y^{\varepsilon}} = 1$.

		FSDT ([8])			LD4-vK			LD4 - Full		
		h/b			h/b			h/b		
N_l	a/b	6.67	10	20	6.67	10	20	6.67	10	20
3	0.5	1.6941	1.8268	1.9301	1.6554	1.8061	1.9246	1.6350	1.7945	1.9211
	1.0	1.7888	1.8971	1.9717	1.7177	1.8597	1.9614	1.7053	1.8529	1.9594
	1.5	1.8100	1.9129	1.9816	1.7272	1.8696	1.9697	1.7186	1.8648	1.9683
	2.0	1.8173	1.9184	1.9852	1.7295	1.8726	1.9725	1.7225	1.8687	1.9714
	2.5	1.8205	1.9208	1.9868	1.7303	1.8738	1.9738	1.7241	1.8704	1.9728
	3.0	1.8222	1.9221	1.9876	1.7306	1.8743	1.9745	1.7249	1.8712	1.9736
5	0.5	3.1502	3.7449	4.2398	2.8650	3.5442	4.1702	2.8274	3.5176	4.1605
	1.0	4.4346	5.2505	5.9052	3.9482	4.9185	5.7926	3.9142	4.8933	5.7832
	1.5	4.8678	5.7569	6.4669	4.3208	5.3865	6.3418	4.2905	5.3631	6.3328
	2.0	4.9727	5.8747	6.5969	4.4454	5.5228	6.4791	4.4139	5.4973	6.4690
	2.5	4.8945	5.7592	6.4506	4.4276	5.4490	6.3468	4.3898	5.4188	6.3351
	3.0	4.8389	5.6889	6.3683	4.3682	5.3707	6.2609	4.3299	5.3415	6.2498
7	0.5	3.6482	4.5102	5.2756	3.4108	4.3343	5.2118	3.3648	4.3004	5.1987
	1.0	5.3083	6.5558	7.6342	4.9153	6.2712	7.5328	4.8697	6.2355	7.5187
	1.5	5.7892	7.1372	8.3016	5.3855	6.8485	8.1992	5.3395	6.8107	8.1838
	2.0	5.7065	6.9679	8.0498	5.3766	6.7366	7.9687	5.3211	6.6909	7.9503
	2.5	5.5977	6.8212	7.8729	5.2586	6.5776	7.7862	5.2040	6.5342	7.7691
	3.0	5.5896	6.8252	7.8903	5.2352	6.5706	7.7998	5.1828	6.5289	7.7833

Table 6: Comparison of buckling factor $k_x^{\varepsilon} = \dfrac{N_x^{\varepsilon} b^2}{E_2 h^3}$ with the exact FSDT solutions of Ref. [8] for FC plates of Material 2 with $E_1/E_2 = 40$ subjected to biaxial compression with $\dfrac{N_x^{\varepsilon}}{N_y^{\varepsilon}} = 1$.

		FSDT ([8])			LD4-vK			LD4 - Full		
		h/b			h/b			h/b		
N_l	a/b	6.67	10	20	6.67	10	20	6.67	10	20
3	0.5	8.7842	13.481	19.870	8.7171	13.3411	19.7750	8.6023	13.2292	19.7096
	1.0	3.3625	3.9586	4.4694	3.2860	3.9145	4.4561	3.2592	3.8963	4.4497
	1.5	2.2640	2.4546	2.5925	2.1815	2.4115	2.5807	2.1689	2.4040	2.5783
	2.0	1.9830	2.1078	2.1926	1.8968	2.0630	2.1803	1.8880	2.0580	2.1788
	2.5	1.8920	2.0009	2.0733	1.8033	1.9547	2.0606	1.7962	1.9507	2.0594
	3.0	1.8570	1.9606	2.0291	1.7666	1.9136	2.0161	1.7603	1.9100	2.0150
5	0.5	9.6989	13.850	18.885	9.5135	13.7809	18.8900	9.4050	13.6596	18.8202
	1.0	5.6131	6.6491	7.4877	5.1817	6.3621	7.3917	5.1330	6.3232	7.3766
	1.5	5.0482	5.9356	6.6453	4.5490	5.5957	6.5299	4.5124	5.5677	6.5193
	2.0	4.9733	5.8751	6.5991	4.4622	5.5253	6.4798	4.4281	5.4991	6.4699
	2.5	4.9360	5.8372	6.5630	4.4419	5.5020	6.4495	4.4068	5.4746	6.4389
	3.0	4.8904	5.7694	6.4755	4.4123	5.4485	6.3677	4.3754	5.4196	6.3565
7	0.5	9.8436	13.785	18.312	9.7159	13.7594	18.3289	9.6090	13.6358	18.2592
	1.0	6.2492	7.6057	8.7666	5.9154	7.3663	8.6812	5.8555	7.3171	8.6615
	1.5	5.8372	7.1622	8.3140	5.4701	6.8917	8.2158	5.4186	6.8507	8.1996
	2.0	5.7500	7.0811	8.2453	5.3999	6.8269	8.1538	5.3473	6.7844	8.1367
	2.5	5.6683	6.9457	8.0510	5.3296	6.7046	7.9658	5.2752	6.6605	7.9480
	3.0	5.6225	6.8704	7.9449	5.2776	6.6238	7.8574	5.2239	6.5807	7.8403

Table 7: Comparison of buckling factor $k_x^\varepsilon = \dfrac{N_x^\varepsilon a^2}{E_2 h^3}$ with two variable refined theory solutions of Ref. [8] for orthotropic plates of Material 3 subjected to biaxial compression with $\dfrac{N_x^\varepsilon}{N_y^\varepsilon} = 1$.

			Two variable refined ([21])			LD4 - Full			LD4 - Full		
	k_x^ε		k_x^ε			k_x^ε associated to $m = 1$			First buckling		
E_1/E_2	a/b	a/h	Boundary conditions			Boundary conditions			Boundary conditions		
			CC	SC	SS	CC	SC	SS	CC	SC	SS
10	0.5	5	7.2377	5.7417	4.0087	6.8094	5.1828	3.9009	3.2675^5	3.0139^4	2.7227^3
		10	16.2061	10.4644	5.9323	15.6287	9.9167	5.8597	6.8392^5	5.6086^4	4.2354^3
		20	23.8339	13.2301	6.7489	23.4837	12.9931	6.7234	10.0314^5	7.3938^4	4.9565^3
		50	27.4847	14.2921	7.0201	27.4067	14.2467	7.0155	11.7212^5	8.1634^4	5.2096^3
	1.0	5	5.6446	4.4633	3.1739	4.7957	3.8160	3.0341	3.3260^2	3.0139^2	2.7547^2
		10	12.1959	7.9337	4.6866	11.0033	7.2738	4.5895	7.0006^2	5.6086^2	4.5650^2
		20	17.3917	9.8817	5.3267	16.7161	9.5958	5.2924	10.3767^2	7.3938^2	5.2924^1
		50	19.7627	10.6137	5.5390	19.6167	10.5589	5.5329	12.1600^2	8.1634^2	5.5329^1
	2.0	5	3.9343	3.3575	2.8549	3.3260	3.0139	2.7547	3.3260^1	3.0139^1	2.7547^1
		10	8.0621	6.0600	4.6718	7.0006	5.6086	4.5650	7.0006^1	5.6086^1	4.5650^1
		20	11.0304	7.6161	5.5687	10.3767	7.3938	5.5229	10.3767^1	7.3938^1	5.5229^1
		50	12.3060	8.2083	5.8861	12.1600	8.1634	5.8774	12.1600^1	8.1634^1	5.8774^1
40	0.5	5	9.7833	8.4941	7.0069	8.6031	7.3479	6.5989	3.4656^5	3.3081^5	3.2011^5
		10	28.8116	22.6976	15.5441	26.9868	20.2794	14.9975	8.2124^6	7.3443^5	6.4966^5
		20	64.1871	40.9916	22.6762	61.9751	38.7935	22.3629	15.1779^7	12.2197^6	9.1643^5
		50	99.5518	53.1946	26.0510	98.6663	52.5689	25.9825	21.6917^7	15.6239^6	10.4590^5
	1.0	5	7.6720	6.5956	5.2892	5.7791	5.0284	4.5677	3.4665^3	3.3611^3	3.2280^2
		10	22.1554	16.9841	11.1291	17.8206	13.5224	10.1074	8.2124^3	7.5105^3	6.5168^2
		20	46.9608	29.1245	15.5343	41.5242	26.0536	14.9681	15.2219^3	12.2197^3	9.2368^2
		50	69.2980	36.5294	17.4859	67.2367	35.6767	17.3648	22.2265^4	15.6239^3	10.5660^2
	2.0	5	5.1918	4.4809	3.6725	3.6413	3.3918	3.2280	3.6243^2	3.3918^1	3.2280^1
		10	14.0497	10.5524	7.2536	9.3964	7.8094	6.5168	8.9554^2	7.8094^1	6.5168^1
		20	26.0470	16.3028	9.6614	20.1003	13.8413	9.2368	15.9245^2	13.8413^1	9.2368^1
		50	34.4402	19.2706	10.6576	32.2567	18.5891	10.5660	22.2265^2	18.1270^2	10.5660^1

Table 8: Buckling factors $k_x = \dfrac{N_x b^2}{E_2 h^3}$ for $[0°/90°/0°]$ plates of Material 2 subjected to biaxial compression with $\dfrac{N_x}{N_y} = 1$

E_1/E_2	a/b	b/h	k_x^σ Boundary conditions						k_x^ε Boundary conditions					
			CC	SC	SS	CF	SF	FF	CC	SC	SS	CF	SF	FF
10	1.0	10	9.5133^2	7.5070^1	4.9095^1	2.2265^1	1.6912^1	1.6613^1	9.5686^2	7.4986^1	4.9095^1	2.2313^1	1.6958^1	1.6667^1
		20	12.8788^2	9.4217^1	5.5082^1	2.3635^1	1.7713^1	1.7290^1	12.9006^2	9.4173^1	5.5082^1	2.3650^1	1.7726^1	1.7305^1
		50	14.4624^2	10.1695^1	5.7063^1	2.4118^1	1.7980^1	1.7491^1	14.4665^2	10.1686^1	5.7063^1	2.4121^1	1.7983^1	1.7493^1
	2.0	10	3.2197^1	2.5302^1	2.1125^1	1.7172^1	1.6730^1	1.6614^1	3.2251^1	2.5354^1	2.1175^1	1.7224^1	1.6782^1	1.6669^1
		20	3.5674^1	2.7036^1	2.2151^1	1.7928^1	1.7440^1	1.7293^1	3.5690^1	2.7051^1	2.2165^1	1.7943^1	1.7454^1	1.7307^1
		50	3.6825^1	2.7575^1	2.2458^1	1.8166^1	1.7657^1	1.7494^1	3.6827^1	2.7577^1	2.2461^1	1.8168^1	1.7660^1	1.7497^1
25	1.0	10	13.8990^2	12.1768^2	8.6820^1	3.8278^1	2.6646^1	2.2536^1	13.9864^2	12.2614^2	8.6820^1	3.8354^1	2.6726^1	2.2582^1
		20	22.6044^2	17.5632^2	10.8768^1	4.2136^1	2.8906^1	2.4649^1	22.6479^2	17.6034^2	10.8768^1	4.2163^1	2.8930^1	2.4664^1
		50	28.4676^2	20.2849^2	11.7320^1	4.3438^1	2.9642^1	2.5430^1	28.4770^2	20.2933^2	11.7320^1	4.3443^1	2.9647^1	2.5433^1
	2.0	10	5.6511^1	4.3908^1	3.5793^1	2.9239^1	2.8603^1	2.6646^1	5.6620^1	4.4008^1	3.5887^1	2.9336^1	2.8702^1	2.6726^1
		20	6.9151^1	4.9865^1	3.9012^1	3.1649^1	3.0983^1	2.8906^1	6.9186^1	4.9897^1	3.9040^1	3.1677^1	3.1013^1	2.8930^1
		50	7.4099^1	5.1897^1	4.0027^1	3.2418^1	3.1736^1	2.9642^1	7.4106^1	5.1902^1	4.0032^1	3.2423^1	3.1741^1	2.9647^1
40	1.0	10	16.6136^2	14.8719^2	11.5031^1	5.2600^1	3.5353^1	2.7476^1	16.7156^2	14.9714^2	11.5031^1	5.2687^1	3.5457^1	2.7529^1
		20	30.1715^2	23.8897^2	15.7560^1	6.0073^1	3.9769^1	3.0996^1	30.2304^2	23.9439^2	15.7560^1	6.0110^1	3.9802^1	3.1015^1
		50	41.6756^2	29.3714^2	17.6586^1	6.2649^1	4.1253^1	3.2275^1	41.6898^2	29.3838^2	17.6586^1	6.2656^1	4.1258^1	3.2278^1
	2.0	10	7.5429^1	5.9724^1	4.8978^1	4.0059^1	3.9215^1	3.5353^1	7.5576^1	5.9860^1	4.9105^1	4.0187^1	3.9349^1	3.5457^1
		20	9.9824^1	7.1612^1	5.5401^1	4.4921^1	4.4098^1	3.9769^1	9.9877^1	7.1659^1	5.5442^1	4.4962^1	4.4140^1	3.9802^1
		50	11.0803^1	7.6027^1	5.7530^1	4.6537^1	4.5714^1	4.1253^1	11.0813^1	7.6035^1	5.7537^1	4.6544^1	4.5721^1	4.1258^1

Table 9: Buckling factors $k_x = \dfrac{N_x b^2}{E_2 h^3}$ for $[0°/90°/0°]$ plates of Material 2 subjected to biaxial compression with $\dfrac{N_x}{N_y} = 2$

E_1/E_2	a/b	b/h	k_x^σ Boundary conditions						k_x^ε Boundary conditions					
			CC	SC	SS	CF	SF	FF	CC	SC	SS	CF	SF	FF
10	1.0	10	14.5510^1	9.7979^1	6.5461^1	3.3141^1	2.7085^1	2.1921^1	14.4803^1	9.7655^1	6.5329^1	3.3127^1	2.7113^1	2.1909^1
		20	20.5709^1	12.2247^1	7.3442^1	3.5128^1	2.8422^1	2.3334^1	20.5289^1	12.2104^1	7.3399^1	3.5129^1	2.8431^1	2.3333^1
		50	23.3357^2	13.1677^1	7.6084^1	3.5844^1	2.8877^1	2.3913^1	23.3354^2	13.1648^1	7.6077^1	3.5845^1	2.8879^1	2.3913^1
	2.0	10	5.2198^1	4.1320^1	3.5209^1	2.9774^1	2.9772^1	2.7085^1	5.2204^1	4.1347^1	3.5250^1	2.9808^1	2.9806^1	2.7113^1
		20	5.7595^1	4.4063^1	3.6918^1	3.1253^1	3.1253^1	2.8422^1	5.7594^1	4.4070^1	3.6930^1	3.1266^1	3.1265^1	2.8431^1
		50	5.9370^1	4.4911^1	3.7431^1	3.1746^1	3.1743^1	2.8877^1	5.9370^1	4.4913^1	3.7433^1	3.1748^1	3.1746^1	2.8879^1
25	1.0	10	22.2108^1	16.2001^1	11.5760^1	5.7047^1	4.2644^1	2.9050^1	22.1276^1	16.1569^1	11.5540^1	5.6967^1	4.2686^1	2.9027^1
		20	36.8220^2	24.5093^1	14.5025^1	6.2563^1	4.6382^1	3.1781^1	36.8374^2	24.4817^1	14.4935^1	6.2560^1	4.6400^1	3.1779^1
		50	45.9675^2	28.8810^1	15.6426^1	6.4426^1	4.7607^1	3.2791^1	45.9683^2	28.8743^1	15.6409^1	6.4427^1	4.7610^1	3.2791^1
	2.0	10	9.2055^1	7.1834^1	5.9655^1	4.9673^1	4.9560^1	4.2644^1	9.2093^1	7.1897^1	5.9738^1	4.9706^1	4.9576^1	4.2686^1
		20	11.1799^1	8.1262^1	6.5020^1	5.4183^1	5.4035^1	4.6382^1	11.1804^1	8.1280^1	6.5045^1	5.4204^1	5.4051^1	4.6400^1
		50	11.9432^1	8.4455^1	6.6712^1	5.5655^1	5.5504^1	4.7607^1	11.9432^1	8.4459^1	6.6716^1	5.5659^1	5.5508^1	14.7610^1
40	1.0	10	26.1573^1	20.1020^1	15.3375^1	7.8512^1	5.6482^1	3.5395^1	26.0706^1	20.0558^1	15.3105^1	7.8318^1	5.6520^1	3.5358^1
		20	49.3174^2	34.4948^1	21.0080^1	8.9203^1	6.3786^1	3.9961^1	49.3449^2	34.4598^1	20.9954^1	8.9188^1	6.3809^1	3.9957^1
		50	67.3695^2	43.9778^1	23.5448^1	9.2873^1	6.6247^1	4.1621^1	67.3716^2	43.9675^1	23.5422^1	9.2874^1	6.6252^1	4.1621^1
	2.0	10	12.3294^1	9.7895^1	8.1630^1	6.7348^1	6.7156^1	5.6482^1	12.3362^1	9.7986^1	8.1745^1	6.7346^1	6.7128^1	5.6520^1
		20	16.1656^1	11.6767^1	9.2335^1	7.6349^1	7.5967^1	6.3786^1	16.1667^1	11.6796^1	9.2372^1	7.6373^1	7.5983^1	6.3809^1
		50	17.8625^1	12.3710^1	9.5883^1	7.9392^1	7.8947^1	6.6247^1	17.8626^1	12.3715^1	9.5890^1	7.9398^1	7.8952^1	6.6252^1

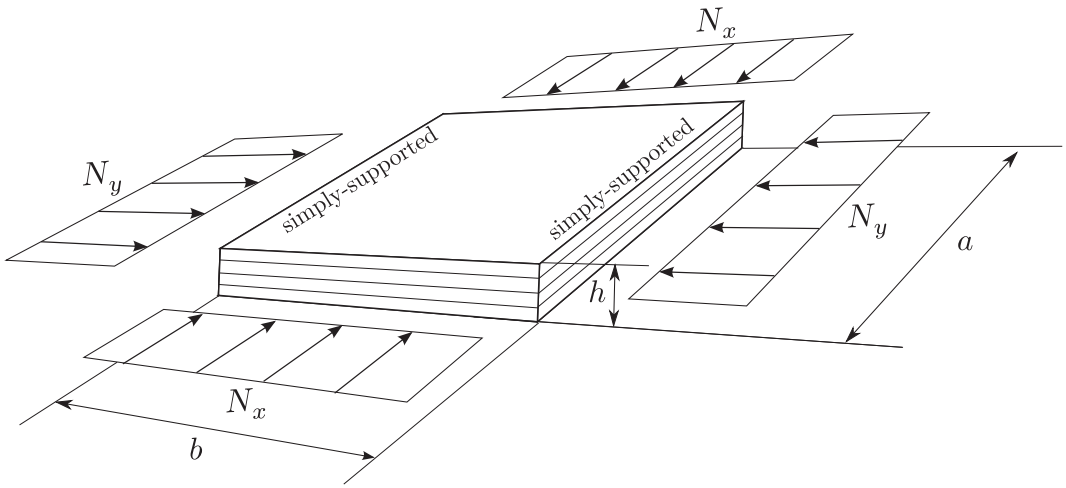

Figure 1: Multilayered plate subjected to biaxial loading.

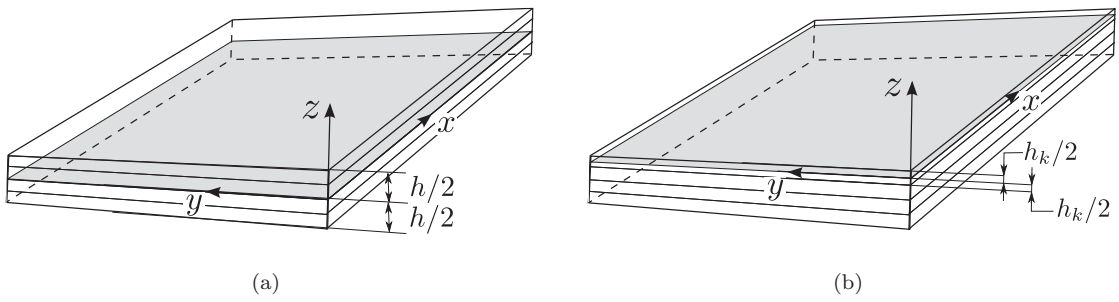

(a) (b)

Figure 2: Reference surfaces and coordinate systems in the two formulations: (a) Equivalent displacement-based theories (EDN), (b) Layerwise displacement-based theory (LDN).